

# REACTIVE POLYMERS AND MICROCAPSULES

# REACTIVE POLYMERS AND MICROCAPSULES

By Mitchell A. Johnson, B. Tech.

A Thesis Submitted to the School of Graduate Studies in Partial Fulfilment  
of the Requirements for the Degree Master of Science

McMaster University © Copyright by Mitchell A. Johnson, 2020

TITLE: REACTIVE POLYMERS AND  
MICROCAPSULES

Author: Mitchell A. Johnson  
B.Tech (Biotechnology)  
McMaster University, Hamilton,  
Ontario, Canada

SUPERVISOR: Dr. Harald Stöver

NUMBER OF PAGES: xiii, 90

## Abstract

In cell encapsulation, cells are embedded within a hydrogel matrix or liquid core capsule, which is designed to isolate donor cells from a patient's immune system. This immunoisolation allows for long term transplant function of therapeutic secreting cells for potential treatment of many hormonal and enzyme deficiency disorders. The work in this thesis focuses on the use and study of reactive polymers for their application in cell application. Incorporation of covalent crosslinking into cell encapsulation by reactive polymers addresses issues of long-term stability seen in conventional alginate – poly(L-lysine) – alginate (APA) capsules, by introducing crosslinks with prolonged stability *in vivo*

Chapter 2 focuses on the use of partially hydrolyzed poly(methyl vinyl ether-alt-maleic anhydride) to form covalently crosslinked shells with surface bound poly(L-lysine) coated onto INS-1E encapsulated alginate beads. The capsules formed were found to maintain *in vitro* stability for 6 weeks and that the coating procedure did not impede INS-1E cellular function, with the encapsulated cells maintaining cell viability and retaining their ability to form cellular clusters in low attachment environments. Additionally, a new fluorescent microscopy-based method was developed to quantify the percentage of protruding cells from the capsules for the first time.

In chapter 3, new Diels Alder reactive polycation copolymers, poly(N,N-dimethyl amino ethyl acrylate-co-Furfuryl acrylamide), was designed and synthesized. The

reactivity ratios measured for the copolymerization were found to be  $r_1 = 1.83$  for N,N-dimethyl amino acrylate and  $r_2 = 0.23$ . These new polycations can be in cell encapsulation to form new covalently crosslinked networks with dieneophile crosslinkers.

## Acknowledgments

I would first like to thank my supervisor Dr. Harald Stöver for being a kind, enthusiastic and supportive mentor as well as for taking a chance on an undergraduate student from a new program and no chemistry background.

I would like to thank all the past and present Stöver group members Jing Zhao, Rachelle Kleinberger, Alison Stewart, Samantha Ros, Sheilan Sinjari, Derrick Hastings, Carl Ellis, Aleks Redžić, and Sean Curtis for their help and friendship during my time here. In particular, I would like to thank Jing Zhao for being the hardest working supervising graduate student during my undergraduate research experience, and both Sam and Sheilan for being always helpful mentoring graduate students during my thesis.

Finally, I would like to especially thank my parents Nancy and James for being constantly supportive.

## Table of Contents

<b>Chapter 1 - Introduction</b> .....	<b>1</b>
1.1 Cell Encapsulation.....	1
1.2 Macro Encapsulation .....	2
1.3 Microencapsulation .....	4
1.4 Microencapsulation Immune Reponses.....	5
1.5 Alginate .....	6
1.6 Alginate bead production.....	9
1.7 Reinforcement of alginate.....	14
1.8 Thesis Focus .....	16
1.9 References .....	17
<b>Chapter 2 - Quantifying Cellular Protrusion in Alginate Capsules with Covalently Crosslinked Shells</b> .....	<b>41</b>
2.1 Abstract .....	41
2.2 Introduction.....	42
2.3 Experimental .....	45
2.3.1 Materials .....	45
2.3.2 Synthesis of 50% hydrolyzed poly(methylvinylether-alt-maleic anhydride), PMM <sub>50</sub> .....	46
2.3.3 Cell Maintenance .....	46
2.3.4 Formation of Calcium Alginate Capsules .....	47
2.3.5 Formation of PLL / PMM <sub>50</sub> Crosslinked Shell.....	48
2.3.6 Measuring Cell Viability using LIVE/DEAD Fluorescence Assay ....	49
2.3.7 Testing Resistance of Crosslinked Shells to Citrate and NaOH.....	50
2.3.8 Synthesis of Rhodamine-labelled Poly-L-Lysine, PLLr .....	50
2.3.9 Confocal Fluorescence Colocalization of INS-1E Cells and Rhodamine-labelled (PLLr) Shells .....	51
2.3.10 Confocal Fluorescence Colocalization of INS-1E Cells with Dextran-f containing continuous media.....	52
2.3.11 Statistical Analysis .....	53

2.4 Results .....	53
2.4.1 Capsule Formation and Properties .....	54
2.4.2 INS-IE Cell Viability.....	56
2.3.3 Radial Position Distribution of INS1E cells by Fluorescence Colocalization.....	59
2.5 Conclusions.....	65
2.6 Conflicts of interest.....	66
2.7 Acknowledgements .....	66
2.8 References .....	66
2.9 Appendix .....	74
<b>Chapter 3 – Diels Alder Reactive Charge-Shifting Polycations.....</b>	<b>77</b>
3.0 Introduction.....	77
3.1 Experimental .....	79
3.11 Materials .....	79
3.12 Synthesis of Furfurylacrylamide (FFAm).....	80
3.13 Reactivity Ratios .....	81
3.2 Results .....	82
3.21 Reactivity Ratios .....	82
3.3 Future Work.....	84
3.4 References .....	85
3.5 Appendix .....	90

## List of Figures

Figure 1.1: Chemical structure of alginate. -----	7
Figure 1.2: Coaxial airflow bead generator. -----	10
Figure 1.3: Electrostatic bead generator. -----	12
Figure 1.4: Islet of Langerhans protruding from microcapsule. -----	13



Figure 2.1: Transmitted light images of tests for covalent crosslinking in Alg-PLL-PMM<sub>50</sub> capsules containing INS-1E cells. A) As-formed capsules in saline; B) Capsules after treatment with 1M Na-citrate to extract calcium; C) Capsules after additional treatment with 0.1M NaOH to disrupt polyelectrolyte complex shells. Scalebar 250 $\mu$ m. -----**Error! Bookmark not defined.**

Figure 2.2: Cell viability: Day 0 INS-1E cells in covalently crosslinked Alg-PLL-PMM<sub>50</sub> capsules with LIVE/DEAD staining: A) equatorial FITC and TRITC confocal sections plus transmitted channel; B) corresponding top-down alpha blending 3D projection of two-channel confocal stack.----- **Error! Bookmark not defined.**

Figure 2.3: Progressive clustering of INS-1E cells in covalently crosslinked Alg-PLL-PMM<sub>50</sub> capsules at days 0, 1, 3, 7 and 14, shown using top-down alpha blending 3D two-channel confocal stacks, and cells stained with Calcein-AM and Ethidium Homodimer -----**Error! Bookmark not defined.**

Figure 2.4: 2D and 3D imaging of INS-1E cells located near the surfaces of covalently crosslinked Alg-PLLr-PMM<sub>50</sub> capsules. A: Two-channel confocal equatorial section of Calcein AM stained INS-1E cells; B: corresponding 3D rendered image; C, D: comparison of two-channel (FITC and TRITC) and single-channel (TRITC) 3D rendered images, respectively, revealing cell-sized areas with lower PLLr concentration in D that correspond with cell positions shown in C. -----**Error! Bookmark not defined.**

Figure 2.5: Protrusion mapping using cell-to-PLLr shell distances in INS-1E containing crosslinked Alg-PLLr-PMM<sub>50</sub> capsules: A) As-obtained two-channel confocal equatorial cross section; B) Binary map derived from thresholding image A in both channels; C) Binary map with cells in contact with PLLr layer marked blue.-----**Error! Bookmark not defined.**

Figure 2.6: Protrusion mapping using cell-to-continuous media distances in INS-1E containing crosslinked Alg-PLLr-PMM<sub>50</sub> capsules: A) Single-channel confocal equatorial section showing LIVE-stained cells and continuous media containing 2 MDa Dex-f (Contrast increased) B) Binary two-channel map obtained from image A by thresholding cells and defining a single pixel-thick layer of continuous media at capsule surface (red circle); C) Alpha blending 3D projection of image B with

protruding cells (cells contacting continuous media) outlined in blue squares.  
Scale bar 100µm. -----**Error! Bookmark not defined.**

Appendix Figure 2.1: Syringe holder with angled air-feed side port, machined from a solid block of carbon-black-loaded Delrin.. **Error! Bookmark not defined.**

Appendix Figure 2.2: Day 14 INS-1E cell cluster stained with Hoechst 3342.  
Scale bar 25µm. .... 75

Appendix Figure 2.3: Inverted brightfield image of Day 42 INS-1E cells (scalebar 500um) ..... 75

Appendix Figure 2.4: Average capsule diameter and percent non-spherical capsules as function of coaxial air flow. Lines are second order polynomial trendlines fitted to the data points to help guide the eye. Experiments were carried out in triplicates, with 30 capsules measured for each sample. .... 76

Appendix Figure 3.1: <sup>1</sup>H NMR of FFAm in CDCl<sub>3</sub> recorded at 600MHz ..... 90

## List of Schemes

Scheme 3.1: Synthesis of FFAm by amidation of reaction of Acryloyl Chloride with furfurylamine.----- 80

Scheme 3.2: NMR scale copolymerization of DMAEA and FFAm ----- 82

Appendix Scheme 2.1: Crosslinking Chemistry for A-PLL-PMM<sub>50</sub> Capsules.---- 74

## List of Tables

Table 2.1: Percentage of cells in contact with PLLr layer, and physically protruding from capsules (n = 3. Dex-f p> 0.05). --**Error! Bookmark not defined.**

Appendix Table 2.1: Cell viabilities of INS-1E encapsulated cells at days 0, 1, and 3. p-values > 0.05 ----- 76

## List of Abbreviations

<b>APA</b>	<b>Alginate-poly-L-lysine-alginate</b>
<b>CaCl<sub>2</sub></b>	<b>Calcium Chloride</b>
<b>Calcein AM</b>	<b>Calcein Acetoxymethyl ester</b>
<b>DCM</b>	<b>Dichloromethane</b>
<b>Dex-<i>f</i></b>	<b>Dextran fluorescein isothiocyanate</b>
<b>DMAEA</b>	<b>Dimethylamino ethyl acrylate</b>
<b>DMSO</b>	<b>Dimethyl Sulfoxide</b>
<b>EDTA</b>	<b>Ethylenediaminetetraacetic acid</b>
<b>FBS</b>	<b>Fetal Bovine Serum</b>
<b>FFAm</b>	<b>Furfuryl Acrylamide</b>
<b>HEPES</b>	<b>4-(2-hydroxyethyl)-1-piperazineethanesulfonic acid</b>
<b>IPN</b>	<b>Interpenetrating Network</b>
<b>NaCl</b>	<b>Sodium Chloride</b>
<b>NaOH</b>	<b>Sodium Hydroxide</b>
<b>NHP</b>	<b>Non-human primate</b>

<b>PAMPs</b>	<b>Pathogen-associate molecular patterns</b>
<b>PEC</b>	<b>Polyelectrolyte Complex</b>
<b>PEG</b>	<b>Poly(ethylene glycol)</b>
<b>PLL</b>	<b>Poly(L-lysine)</b>
<b>PLLr</b>	<b>Poly(L-lysine) rhodamine</b>
<b>PLO</b>	<b>Poly(L-ornithine)</b>
<b>PMM50</b>	<b>Poly(methyl vinyl ether-alt-maleic anhydride) 50% hydrolyzed</b>
<b>PMV</b>	<b>Poly(methacrylic acid-co-2-vinyl-4,4-dimethylazalactone)</b>
<b>PTFE</b>	<b>Poly(tetrafluoroethylene)</b>
<b>RITC</b>	<b>Rhodamine isothiocyanate</b>
<b>RPMI</b>	<b>Roswell Park Memorial Institute Medium</b>
<b>TEA</b>	<b>Triethyl amine</b>
<b>TLR</b>	<b>Toll-like receptors</b>

## **Declaration of Academic Achievement**

### **Chapter 2**

Preliminary cell encapsulation experimental design and cell culture was done by Ali Abu Helal, Nicholas A.D. Burke, Shanna Shi, Rachelle Kleinberger, Ahmed Ayyash, and Nicole Latchminarine. Published experimental procedures and results were design and performed by me. The manuscript was cowritten by Dr. Stover and I with edits from Dr. Alison Holloway

### **Chapter 3**

I designed and performed all the monomer and copolymer synthesis. NMR interpretation and reactivity ratio determination were done by me with guidance from Samantha Ros. I wrote the manuscript with guidance and edits from Dr. Stover.

## **Chapter 1 - Introduction**

### **1.1 Cell Encapsulation**

Currently, the treatment methods of many hormonal and enzyme deficiency disorders are limited to frequent administrations of therapeutic peptides or hormones as in the case of insulin for Type 1 diabetes. To address the need of continuous drug delivery for chronic treatments, new polymeric drug delivery methods have been developed. Ideally, these systems would be able to achieve targeted local drug delivery with tailored long-term continuous delivery of therapeutic agents.<sup>1-4</sup> Another approach is to use cell-based therapies. These new treatments utilize therapeutic secreting cells to provide controlled release of targeted therapeutic agents. The benefit of using therapeutic cells is that they can provide sustained as well as bio-feedback controlled release, and avoid the potential sudden burst release of high drug doses upon administration, erosion or breakage of polymeric drug delivery systems.<sup>5,6</sup>

Over the past few decades cell encapsulation has been extensively researched for cell-based therapies. In cell encapsulation, cells are immobilized within a semipermeable material that acts as barrier to hide donor cells from a patient's immune system, creating physical separation of donor cells from immune cells as well as excluding cytotoxic larger immunological molecules such as antibodies and cytokines.<sup>7</sup> The concept of cell encapsulation was first demonstrated in 1933 by Bisceglie when it was shown that encapsulated mouse

tumor cells implanted in a pig remained viable and avoided immune rejection.<sup>8</sup>

The concept of cell encapsulation as source of artificial organs was later introduced by Chang in 1964.<sup>9</sup>

The potential viability of cell encapsulation as a new treatment method was demonstrated in 1980 by Sun and Lim.<sup>10</sup> In this seminal paper, encapsulated xenogenic pancreatic islets were shown to maintain blood glucose levels for several weeks in diabetic rat models, with unencapsulated islets returning to pretreatment levels only after a few days. Cell encapsulation research has since been expanded to a variety of other diseases including hemophilia,<sup>11</sup> dwarfisms,<sup>12</sup> central nervous system insufficiencies,<sup>13</sup> and liver and kidney failure.<sup>14,15</sup>

## **1.2 Macro Encapsulation**

Research towards designing cell encapsulation devices has been focused on two approaches: macro- and micro-encapsulation systems. Macro encapsulation devices are either extravascular or intravascular in nature, and have been designed in a variety of structures such as hollow fibers,<sup>16,17</sup> macrocapsules,<sup>18,19</sup> pouches,<sup>20</sup> and sheets.<sup>21</sup> Extravascular devices rely on diffusive transport for nutrient and oxygen supply to the encapsulated cells and are typically implanted into low risk surgical sites, either subcutaneously or in the peritoneal cavity. Due to their reliance on diffusive transport extravascular microencapsulation devices often face issues of hypoxia and necrosis for cells

located towards the center of the device, which limits cell densities and introduces significant dead volume. Some macrocapsule devices incorporate oxygen supply systems to help maintain beta cells. Beta-O<sub>2</sub> is an implanted device developed consisting of cells encapsulated in an alginate gel around a gas cavity that has an access port to an external oxygen supply and has shown in small animal studies to maintain islet function over 90 days.

To overcome these challenges new devices have been designed that promote angiogenesis to vascularize the transplant site. TheraCyte is a planar pouch that has a double membrane structure developed by Baxter Healthcare. The membranes are made of polytetrafluoroethylene (PTFE) with differing thicknesses and pore sizes. The outer membrane has a thickness 15  $\mu\text{m}$  and a pore size of 5  $\mu\text{m}$  and promotes angiogenesis, the inner membrane is 30  $\mu\text{m}$  thick with a pore size of 0.4  $\mu\text{m}$  for immune isolation.<sup>20,22,23</sup> It was found that the 5  $\mu\text{m}$  pores of the outer membrane were found to have an 80-100 fold increase in vascularization in to smaller pored membranes, and this increased vascularization is maintained when the two membranes are combined, leading to a highly vascularized device that maintains immunoisolation.<sup>20</sup> Implanted rat islets in the TheraCyte device were found to remain functional for 4 weeks in immunocompromised mice and neonatal porcine islets transplanted into non-obese diabetic mice showed reversal of diabetes for 16 weeks.<sup>24,25</sup> In non-human primate (NHP) models allogenic NHP islets remained viable for up to 12



months.<sup>26</sup> This work is continued by ViaCyte, with early clinical trials showing mixed results due to fibrosis.

### **1.3 Microencapsulation**

Microencapsulation is similar to extravascular macro encapsulation devices in that it depends on diffusive transport of oxygen and nutrients for cellular function. In contrast to macro encapsulation, the smaller size of microcapsules results in a higher surface area to volume ratio that improves mass transport of oxygen and nutrients, reducing hypoxia and necrosis observed in macro encapsulation.<sup>27</sup> Microcapsules are typically spherical hydrogel beads or liquid core capsules with a semipermeable outer membrane, with diameters between 100 and 1500  $\mu\text{m}$ .

Over the past few decades, microencapsulation has shown promising results in pre-clinical trials. Lim and Sun showed blood glucose regulation for up to 3 weeks in diabetic rat models with pancreatic islets encapsulated in alginate – poly-L-lysine – alginate (APA) beads.<sup>10</sup> In a non-human primate study, 7 out of 9 diabetic monkeys treated with porcine islets encapsulated in APA beads showed insulin independence for 120 to 804 days.<sup>28</sup> A human trial conducted in 1994 showed insulin independence for 9 months in a 30 year old insulin-dependent diabetic patient when transplanted with cadaveric human islets encapsulated in alginate, while maintaining a low daily dose immunosuppression regime of cyclosporin and azathiophene.<sup>29</sup> In 2006, the first non-immuno-suppressed human trial was carried out. Two type 1 diabetic patients received human islets

encapsulated in calcium alginate – poly-L-ornithine – alginate beads, into the peritoneal cavity. While the patients did not achieve insulin independence; there was a decrease in required daily exogenous insulin, reduction in mean blood glucose levels, and elimination of weekly severe hypoglycemia events.<sup>30</sup> In another study in 2016, eight non-immunosuppressed type 1 diabetic patients received encapsulated neonatal porcine islets into the peritoneal cavity. There was an observed significant reduction in hypoglycemia events for > 600 days, but there was minimal reduction in required exogenous insulin.<sup>31</sup> In similar studies, significant insulin dose reduction or insulin independence were rare.<sup>32–34</sup>

#### **1.4 Microencapsulation Immune Responses**

Despite significant research progress and promising animal and immunosuppressed human studies, there has been limited success in clinical trials with non-immunosuppressed humans, which suggest that immuno-isolation remains a key issue. The immune response to microcapsules can be categorized into three sequential steps: acute inflammation, chronic inflammation and lastly granulation tissue development.<sup>32,34–37</sup> The acute inflammatory response is characterized by protein and immunoglobulin adsorption upon transplantation and appearance of granulocytic neutrophils carrying chemokines at the site. After this step, the chronic inflammatory response starts with the appearance of monocytes and lymphocytes, which leads to the appearance of macrophages and fibroblasts

and granulation tissue development. The macrophages adhere to the surface of the capsules and secrete proteins that modulate fibrosis by stimulating fibroblasts, resulting in fibrotic capsule formation around the microcapsules, which reduces nutrient access to encapsulated cells and eventual loss of viable cells.<sup>38-40</sup>

Protein adsorption is one of the key steps that leads to the foreign body response towards implanted biomaterials. The type, amount and conformations of the proteins adsorbed onto the surface all have an effect on the response as these dictate the adhesion of monocytes and macrophages to the materials surface.<sup>41-43</sup> A significant factor in the degree of amount and denaturation of adsorbed proteins is surface hydration. Hydrophilic surfaces have been found to have low degrees of protein denaturation and adsorption in comparison to hydrophobic surfaces.<sup>44-47</sup> The majority of microencapsulation systems are made of hydrogels, mainly alginate.<sup>5</sup> Hydrogels are water swollen crosslinked polymer networks made of hydrophilic polymers.<sup>48-50</sup> Despite the high degree hydrophilicity, plasma protein adsorption is still present and remains a key barrier to successful long-term function of implanted microencapsules.<sup>50-53</sup>

## **1.5 Alginate**

Alginate is an anionic polysaccharide biopolymer extracted from algae consisting of (1-4)-linked  $\beta$ -D-mannuronate (M) and  $\alpha$ -L-gulonate (G) residues with a varying block copolymer sequence of M, G, and GM blocks.

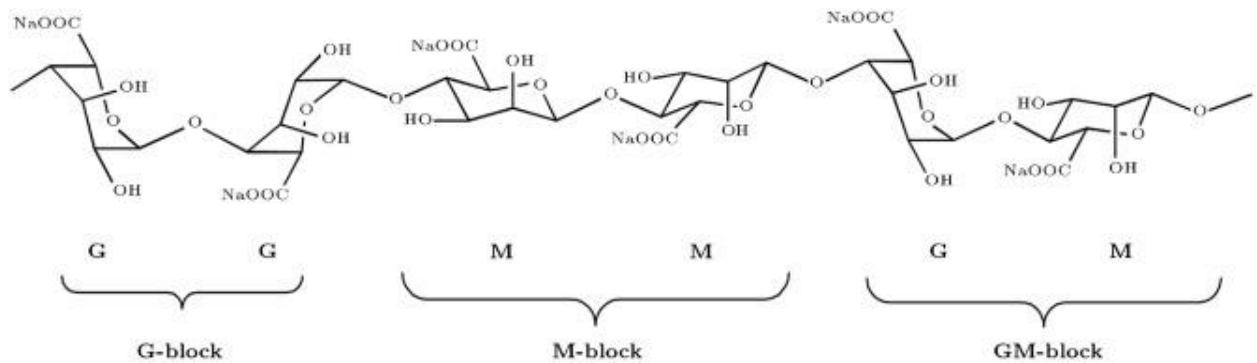


Figure 1.1: Chemical structure of alginate.<sup>54</sup>

The ratios and sequence of the G, M, and GM blocks is found to vary with the source of the alginate and this variation effects the mechanical prosperities of the resulting hydrogels formed. Alginate is capable of forming hydrogels by coordination of guluronic acid units to multivalent cations, such as  $\text{Ca}^{2+}$ , and dimerizing polymer chains leading to hydrogel network formation referred to as the egg-box model.<sup>55-58</sup>

Alginate has been the most used material for microencapsulation due to its low cytotoxicity and mild gelation conditions. It is capable of quickly forming hydrogels under physiological pH, osmolarity and temperature, allowing for simple encapsulation of cells by dropping a solution of alginate containing a suspension of cells into a collection bath containing an aqueous solution of crosslinking ions. Alginate can be crosslinked by a variety of multivalent cations

such as  $\text{Ca}^{2+}$ ,  $\text{Ba}^{2+}$ ,  $\text{Cu}^{2+}$ ,  $\text{Ce}^{3+}$ , and  $\text{Fe}^{3+}$ ,<sup>59–62</sup> with  $\text{Ca}^{2+}$  and  $\text{Ba}^{2+}$  being used for cell encapsulation due to cytotoxicity of other cations. Gelation by  $\text{Ba}^{2+}$  forms more mechanically strong alginate gels due to its higher binding affinity to alginate compared to  $\text{Ca}^{2+}$ .<sup>63,64</sup>

A significant drawback for using alginate as a material for cell encapsulation is that there is significant batch to batch variability in the G:M ratio affecting biocompatibility and mechanical properties of the resulting gel. Higher G content alginates form stronger and stiffer gels compared to lower G content alginates.<sup>65</sup> As well, the G:M ratio affects the physiochemical changes *in vivo* in the properties of implanted capsules. In 2012, Paul de Vos et al showed that alginate-PLL capsules with different degrees of G content can have significant differences in inflammatory response. High G content and intermediate G content alginate-PLL capsules with near identical physiochemical properties were implanted into rats. It was found that the high G content capsules produce a larger inflammatory response, this was attributed to more PLL detachment *in vivo* resulting in a higher positive charge density surface, increasing protein binding.<sup>35,66</sup>

Alginate has also been found to contain many biological impurities such as endotoxins, proteins, and polyphenols that contribute to inflammation, fibrotic overgrowth and cell necrosis. Extensive purification methods have been developed, but there are still residual contaminants.<sup>67–69</sup> Endotoxins are highly immunogenic impurities containing pathogen-associated molecular patterns

(PAMPs). PAMPs are molecular motifs that are recognised by toll-like receptors (TLR) found in the cells of innate immune system.<sup>70</sup> As a result of these issues, new synthetic polymers that can be synthesized without batch-to-batch variability and biological contaminants have potential to be the next generation of materials used in cell encapsulation.

### **1.6 Alginate bead production**

While the materials used for cell encapsulation are important for immunisation, the size and morphology of the resulting beads are also of significant importance for the successes of cell encapsulation. The size of the beads has a large effect on the availability of nutrients to the encapsulated cells, as with smaller sizes there is improved diffusive nutrient exchange due to the increase in the surface area to volume ratio. It has also recently been reported that the size of the beads can have an effect on the degree of immune response. Early work has showed that smaller capsules have improved biocompatibility compared to larger ones. This was attributed to improved oxygenation resulting in less cellular death.<sup>71</sup> In later work comparing empty capsules of 0.350mm and 1.250mm diameter it was found that the smaller capsules still showed better biocompatibility.<sup>72</sup> In contrast to this, recent work by Anderson et al showed the opposite trend. When a series of increasing size  $Ba^{+2}$  alginate beads from 0.3mm to 1.9mm were implanted into C57BL/6 mice. It was found with an increase in size there was a decrease in fibrotic overgrowth on the explanted beads. This trend was still observed when the total surface area of implanted

beads was normalized as well as when comparing the effect of size with different spherical materials such as, stainless steel, glass, and polystyrene.<sup>73</sup>

Despite conflicting results on what is considered the “best” performing bead size, the data demonstrate the importance of being able to produce spherical beads at targeted sizes with low dispersity. Conventional methods for bead production in cell microencapsulation have been based on the droplet extrusion of a sodium alginate solution containing a suspension of cells into a crosslinking gelling bath. One of the early methods for controlling droplet size is a coaxial air flow to shear off droplets.

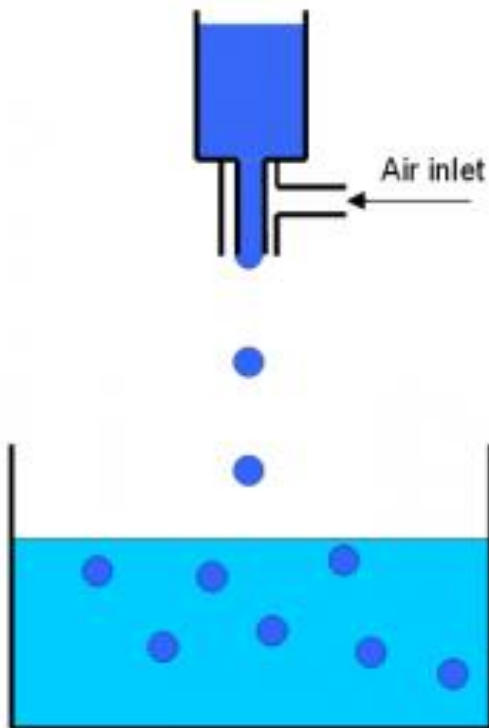


Figure 1.2: Coaxial airflow bead generator.<sup>74</sup>

Beads produced by this method are generally in the range of 0.500mm to 1.0mm in diameter.<sup>75-78</sup> Attempts to reach < 0.500mm diameters often result in bead imperfections such striations and craters as well as droplet fragmentation due to higher air flow rates.<sup>79,80</sup> To achieve smaller sizes of > 0.150mm encapsulators that use an electrostatic potential between the droplet and gelling bath have been developed. The applied voltage, commonly in the range of 1 to 10 kV, reduces droplet size as voltage the increases up to a critical voltage where a taylor cone forms at the nozzle tip, ejecting droplets.<sup>81-83</sup> Beads made by this method are generally more narrow disperse, spherical and have fewer imperfections then those formed by air-shearing.<sup>72</sup>



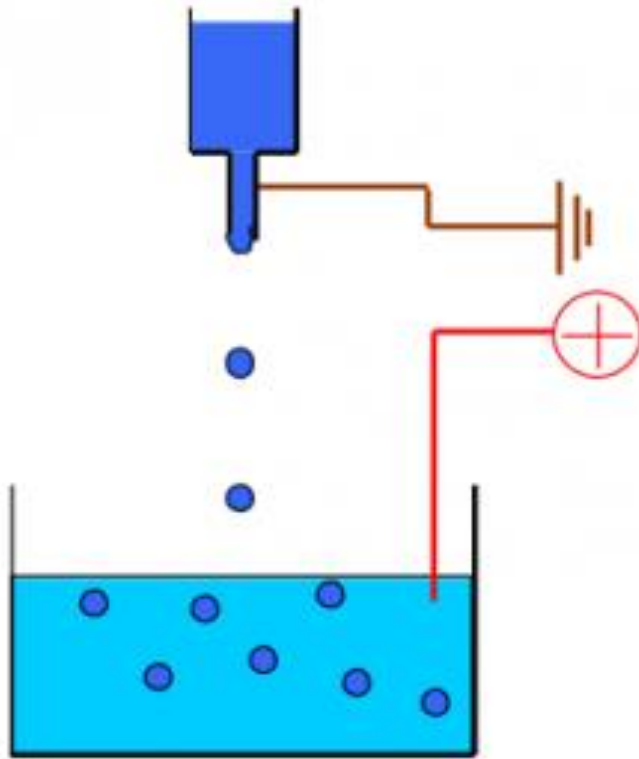


Figure 1.3: Electrostatic bead generator.<sup>74</sup>

Droplet-based microfluidics have been used for forming capsules at < 0.100mm range. There are two general approaches for forming alginate gels with microfluidics, either an external or internal gelling ion source. In the external approach, alginate droplets are formed in a microchannel. These droplets are then met with an external stream of aqueous solution containing crosslinking ions.<sup>84,85</sup> The internal approach uses a water-in-oil emulsion in which aqueous droplets of sodium alginate containing  $\text{CaCO}_3$  nanoparticles are formed in an acidified oil sheath phase. The acidified oil phase forms in situ calcium ions that crosslink the droplet.<sup>86</sup> The benefit of being able to form monodisperse aqueous droplets in a water-in-oil emulsion also allows the use of slower kinetic

crosslinking to form hydrogels. Such as Thiol-Michael addition of acrylated PEG polymers.<sup>87</sup> Major limitations with microfluidics for cell encapsulation is that the microfluidic devices can be prone to clogging, the high injection pressures of viscous polymeric solutions in microchannels can lead to debonding, and the rate of capsule production is lower than droplet extrusion based methods.<sup>88</sup>

A significant problem found in all these bead production methods is the presence of a percentage of the beads having cells protruding from the surface.

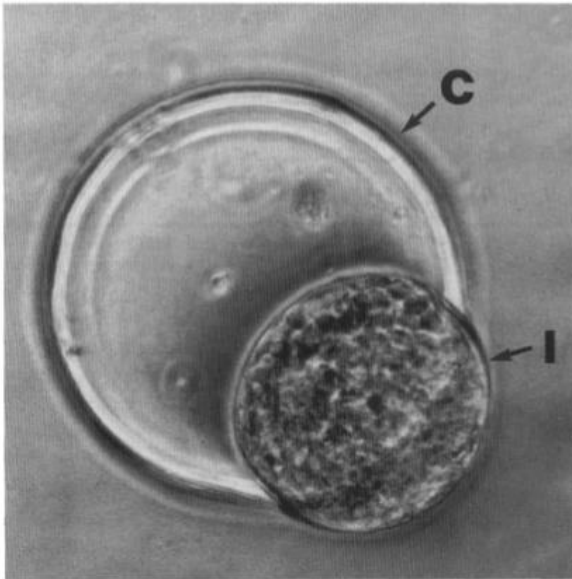


Figure 1.4: Islet of Langerhans protruding from microcapsule.<sup>72</sup>

This protrusion is problematic because it can lead to an immune response as well as capsule rupture.<sup>89,90</sup> Double encapsulations and core-shell encapsulations in which a second additive outer layer of alginate gel is added to the capsule have been developed and have shown to inhibit capsule rupture due

to growing protruding cells.<sup>90,91</sup> These additive layers introduce a significant amount of dead volume that may limit nutrient diffusion. Some single-cell encapsulations with microfluidics have been found to center cells prior to gelation, preventing protrusion.<sup>92,93</sup>

### **1.7 Reinforcement of alginate**

Calcium alginate gels are both too permeable for immuno-isolation and suffer from poor long-term stability *in vivo*. This poor stability is due to ion exchange of monovalent cations for crosslinking multivalent cations that degrades the gel network. To both increase long-term stability and reduce permeability, polycations are often used as coatings. Polycations can be used to complex with the polyanionic alginate by diffusing into the alginate gel and forming a polyelectrolyte complex (PEC).<sup>94</sup> This complexation can be often limited to near the capsule surface, producing a long-term membrane that improves stability and decreases porosity of the capsules.<sup>95</sup>

Despite ease of use and improved capsule performance there are significant issues associated with the use of polycations. Polycations are generally both cytotoxic and immunogenic. They are capable of disrupting cellular membranes by binding to the anionic phospholipid part of cellular membranes.<sup>96,97</sup> Additionally, the cationic charge patches can be pro-inflammatory and can bind serum proteins, leading to a foreign body response.<sup>98,99</sup> As well, PECs themselves can be hydrophobic which also causes significant cellular attachment and protein adsorption.<sup>100</sup>

The polycations typically used in microencapsulation have been based on poly amino acids, with poly-L-lysine (PLL) or poly-L-ornithine (PLO) being the most frequently used.<sup>101</sup> Many new synthetic polycations have been looked at as ways to reduce the adverse effects associated with polycations. Both block and graft copolymers of PLL with poly(ethylene glycol) (PEG) have been shown to have improved biocompatibility and less protein fouling than conventional PLL coatings, but also suffer poorer complexation due steric hinderance from the PEG chains.<sup>102,103</sup> Additionally, the appearance of anti-PEG antibodies has the potential for deleterious effects when using this materials for immunoisolation.<sup>104</sup> Synthetic copolymers of cationic monomers with either neutral, anionic or zwitterionic comonomers have been shown to maintain efficient complexation with alginate while having a reduced cationic charge density.<sup>105,106</sup> As well, “*charge-shifting*” polycations containing reactive cationic groups that can be converted to anionic groups have also been studied.<sup>107</sup>

While polycations used in alginate coatings are complexed and thus have reduced exposed cationic charges, the complexes formed on surface of the capsules are heterogeneous and result in patches of exposed cationic charges at the surface. To address this, secondary coatings with polyanions, commonly sodium alginate, have been used to complex with these exposed cationic charges.<sup>5</sup> A problem with this approach is the *in vivo* loss of the secondary polyanionic coating, that re-exposes these charges.<sup>108</sup> As a result, significant research has been done on developing new synthetic polyanions to replace the

final polyanion coating that are capable of covalently crosslinking with the polycation coating.<sup>109-112</sup> Gardner et al. showed in a C57/b17 mouse study that capsules coated with reactive polyanions poly(methacrylic acid-co-2-vinyl-4,4-dimethylazlactone) (PMV) or partial hydrolyzed poly(methyl vinyl ether-alt-maleic anhydride) (PMM50) had significantly less fibrotic overgrowth on explanted capsules after 6 weeks *in vivo* compared to APA capsules, with PMM50 capsules showing only 2.5% fibrotic overgrowth.<sup>113</sup>

Other approaches that avoid using polycations to improve capsule stability and reduce permeability are using alternative gelling ions, such as Ba<sup>2+</sup> in place of Ca<sup>2+</sup>, or forming interpenetrating gel networks (IPNs). IPNs are secondary crosslinked gel networks within a hydrogel. IPNs based on synthetic hydrogels crosslinked within calcium alginate beads have been explored as a method of tuning the physiochemical properties of calcium alginate beads while also providing encapsulated cells a long term permanent hydrogel matrix.<sup>114-117</sup> Mesenchymal stem cells encapsulated in alginate microspheres with a PEG IPN crosslinked by vinyl sulfone chemistry were successful in reducing liver fibrosis in immunocompetent mice, demonstrating improved immuno-isolation function as well as maintenance of cellular function.<sup>118</sup>

## **1.8 Thesis Focus**

The focus of this thesis is the exploration of reactive polymers and new method development for cell encapsulation. In chapter 2, INS-1E cells, an immortalized rat beta cell line, were encapsulated in capsules with covalently

crosslinked shells using PMM50 chemistry. The effect of the encapsulation and coating process on cellular function was measured. The results showed that the encapsulated cells remained viable over 14 days, and that the INS1e cells maintain their ability to form cellular clusters in low attachment environments. Additionally, a fluorescence-based image processing technique was developed to measure and quantitate the degree of cellular protrusion for the first time. Chapter 3 presents the preliminary design and synthesis of new Diels-Alder crosslinkable charge-shifting polycations based on the copolymerization of a furan functional acrylamide monomer with N,N-(dimethylamino) ethyl acrylate.

## 1.9 References

- (1) Uhrich, K. E.; Cannizzaro, S. M.; Langer, R. S.; Shakesheff, K. M. Polymeric Systems for Controlled Drug Release. *Chem. Rev.* **1999**, *99* (11), 3181–3198. <https://doi.org/10.1021/cr940351u>.
- (2) Richardson, T. P.; Peters, M. C.; Ennett, A. B.; Mooney, D. J. Polymeric System for Dual Growth Factor Delivery. *Nat. Biotechnol.* **2001**, *19* (11), 1029–1034. <https://doi.org/10.1038/nbt1101-1029>.
- (3) Sun, Q.; Chen, R. R.; Shen, Y.; Mooney, D. J.; Rajagopalan, S.; Grossman, P. M. Sustained Vascular Endothelial Growth Factor Delivery Enhances Angiogenesis and Perfusion in Ischemic Hind Limb. *Pharm. Res.* **2005**, *22* (7), 1110–1116. <https://doi.org/10.1007/s11095-005-5644-2>.

- (4) Champion, J. A.; Katare, Y. K.; Mitragotri, S. Particle Shape: A New Design Parameter for Micro- and Nanoscale Drug Delivery Carriers. *Journal of Controlled Release*. August 16, 2007, pp 3–9.  
<https://doi.org/10.1016/j.jconrel.2007.03.022>.
- (5) Murua, A.; Portero, A.; Orive, G.; Hernández, R. M.; de Castro, M.; Pedraz, J. L. Cell Microencapsulation Technology: Towards Clinical Application. *Journal of Controlled Release*. Elsevier December 8, 2008, pp 76–83.  
<https://doi.org/10.1016/j.jconrel.2008.08.010>.
- (6) Orive, G.; Hernández, R. M.; Gascón, A. R.; Calafiore, R.; Chang, T. M. S.; Vos, P. De; Hortelano, G.; Hunkeler, D.; Lacík, I.; Shapiro, A. M. J.; et al. Cell Encapsulation: Promise and Progress. *Nat. Med.* **2003**, 9 (1), 104–107. <https://doi.org/10.1038/nm0103-104>.
- (7) Orive, G.; Hernández, R. M.; Rodríguez Gascón, A.; Calafiore, R.; Chang, T. M. S.; De Vos, P.; Hortelano, G.; Hunkeler, D.; Lacík, I.; Pedraz, J. L. History, Challenges and Perspectives of Cell Microencapsulation. *Trends in Biotechnology*. Elsevier Ltd February 2004, pp 87–92.  
<https://doi.org/10.1016/j.tibtech.2003.11.004>.
- (8) Bisceglie, V. Über Die Antineoplastische Immunität - I. Mitteilung. Heterologe Einpflanzung von Tumoren in Hühnerembryonen. *Z. Krebsforsch.* **1934**, 40 (1), 122–140. <https://doi.org/10.1007/BF01636399>.
- (9) Chang, T. M. S. Semipermeable Microcapsules. *Science (80- )*. **1964**, 146

- (3643), 524–525. <https://doi.org/10.1126/science.146.3643.524>.
- (10) Lim, F.; Sun, A. M. Microencapsulated Islets as Bioartificial Endocrine Pancreas. *Science* **1980**, *210* (4472), 908–910.
- (11) Liu, H. W.; Ofosu, F. A.; Chang, P. L. Expression of Human Factor IX by Microencapsulated Recombinant Fibroblasts. *Hum. Gene Ther.* **1993**, *4* (3), 291–301. <https://doi.org/10.1089/hum.1993.4.3-291>.
- (12) Chang, P. L.; Shen, N.; Westcott, A. J. Delivery of Recombinant Gene Products with Microencapsulated Cells In Vivo. *Hum. Gene Ther.* **1993**, *4* (4), 433–440. <https://doi.org/10.1089/hum.1993.4.4-433>.
- (13) Aebischer, P.; Goddard, M.; Signore, A. P.; Timpson, R. L. Functional Recovery in Hemiparkinsonian Primates Transplanted with Polymer-Encapsulated PC12 Cells. *Exp. Neurol.* **1994**, *126* (2), 151–158. <https://doi.org/10.1006/exnr.1994.1053>.
- (14) Cieslinski, D. A.; David Humes, H. Tissue Engineering of a Bioartificial Kidney. *Biotechnol. Bioeng.* **1994**, *43* (7), 678–681. <https://doi.org/10.1002/bit.260430718>.
- (15) Chang, T. M. Hybrid Artificial Cells: Microencapsulation of Living Cells. *ASAIO J.* **1992**, *38* (2), 128–130.
- (16) Lacy, P. E.; Hegre, O. D.; Gerasimidi-Vazeou, A.; Gentile, F. T.; Dionne, K. E. Maintenance of Normoglycemia in Diabetic Mice by Subcutaneous



- Xenografts of Encapsulated Islets. *Science (80-. )*. **1991**, *254* (5039), 1782–1784. <https://doi.org/10.1126/science.1763328>.
- (17) Sullivan, S. J.; Maki, T.; Borland, K. M.; Mahoney, M. D.; Solomon, B. A.; Muller, T. E.; Monaco, A. P.; Chick, W. L. Biohybrid Artificial Pancreas: Long-Term Implantation Studies in Diabetic, Pancreatectomized Dogs. *Science (80-. )*. **1991**, *252* (5006), 718–721. <https://doi.org/10.1126/science.2024124>.
- (18) Kessler, L.; Pinget, M.; Aprahamian, M.; Dejardin, P.; Damge, C. In Vitro and in Vivo Studies of the Properties of an Artificial Membrane for Pancreatic Islet Encapsulation. *Horm. Metab. Res.* **1991**, *23* (7), 312–317. <https://doi.org/10.1055/s-2007-1003685>.
- (19) Kessler, L.; Legeay, G.; Jesser, C.; Damgé, C.; Pinget, M. Influence of Corona Surface Treatment on the Properties of an Artificial Membrane Used for Langerhans Islets Encapsulation: Permeability and Biocompatibility Studies. *Biomaterials* **1995**, *16* (3), 185–191. [https://doi.org/10.1016/0142-9612\(95\)92116-n](https://doi.org/10.1016/0142-9612(95)92116-n).
- (20) Brauker, J. H.; Carr-Brendel, V. E.; Martinson, L. A.; Crudele, J.; Johnston, W. D.; Johnson, R. C. Neovascularization of Synthetic Membranes Directed by Membrane Microarchitecture. *J. Biomed. Mater. Res.* **1995**, *29* (12), 1517–1524. <https://doi.org/10.1002/jbm.820291208>.
- (21) Lamb, M.; Storrs, R.; Li, S.; Liang, O.; Laugenour, K.; Dorian, R.;

- Chapman, D.; Ichii, H.; Imagawa, D.; Foster, C.; et al. Function and Viability of Human Islets Encapsulated in Alginate Sheets: In Vitro and in Vivo Culture. In *Transplantation Proceedings*; 2011; Vol. 43, pp 3265–3266. <https://doi.org/10.1016/j.transproceed.2011.10.028>.
- (22) Lee, S. H.; Hao, E.; Savinov, A. Y.; Geron, I.; Strongin, A. Y.; Itkin-Ansari, P. Human  $\beta$ -Cell Precursors Mature into Functional Insulin-Producing Cells in an Immunoisolation Device: Implications for Diabetes Cell Therapies. *Transplantation* **2009**, *87* (7), 983–991. <https://doi.org/10.1097/TP.0b013e31819c86ea>.
- (23) Trivedi, N.; Steil, G. M.; Colton, C. K.; Bonner-Weir, S.; Weir, G. C. Improved Vascularization of Planar Membrane Diffusion Devices Following Continuous Infusion of Vascular Endothelial Growth Factor. *Cell Transplant.* **2000**, *9* (1), 115–124. <https://doi.org/10.1177/096368970000900114>.
- (24) Sörenby, A. K.; Kumagai-Braesch, M.; Sharma, A.; Hultenby, K. R.; Wernerson, A. M.; Tibell, A. B. Preimplantation of an Immunoprotective Device Can Lower the Curative Dose of Islets to That of Free Islet Transplantation-Studies in a Rodent Model. *Transplantation* **2008**, *86* (2), 364–366. <https://doi.org/10.1097/TP.0b013e31817efc78>.
- (25) Elliott, R. B.; Escobar, L.; Calafiore, R.; Basta, G.; Garkavenko, O.; Vasconcellos, A.; Bambra, C. Transplantation of Micro- and

Macroencapsulated Piglet Islets into Mice and Monkeys. In *Transplantation Proceedings*; Elsevier USA, 2005; Vol. 37, pp 466–469.

<https://doi.org/10.1016/j.transproceed.2004.12.198>.

- (26) Sasikala, M.; Rao, G. V.; Vijayalakshmi, V.; Pradeep, R.; Pothani, S.; Kumar, P. P.; Gaddipati, R.; Sirisha, G.; Cheemalakonda, R.; Tandan, M.; et al. Long-Term Functions of Encapsulated Islets Grafted in Nonhuman Primates without Immunosuppression. *Transplantation* **2013**, *96* (7), 624–632. <https://doi.org/10.1097/TP.0b013e31829e26cf>.
- (27) de Vos, P.; Andersson, A.; K. Tam, S.; M. Faas, M.; P. Halle, J. Advances and Barriers in Mammalian Cell Encapsulation for Treatment of Diabetes. *Immunol. Endocr. Metab. Agents Med. Chem.* **2006**, *6* (2), 139–153. <https://doi.org/10.2174/187152206776359948>.
- (28) Sun, Y.; Ma, X.; Zhou, D.; Vacek, I.; Sun, A. M. Normalization of Diabetes in Spontaneously Diabetic Cynomologus Monkeys by Xenografts of Microencapsulated Porcine Islets without Immunosuppression. *J. Clin. Invest.* **1996**, *98* (6), 1417–1422. <https://doi.org/10.1172/JCI118929>.
- (29) Soon-Shiong, P.; Heintz, R. E.; Merideth, N.; Yao, Q. X.; Yao, Z.; Zheng, T.; Murphy, M.; Moloney, M. K.; Schmehl, M.; Harris, M. Insulin Independence in a Type 1 Diabetic Patient after Encapsulated Islet Transplantation. *Lancet (London, England)* **1994**, *343* (8903), 950–951. [https://doi.org/10.1016/s0140-6736\(94\)90067-1](https://doi.org/10.1016/s0140-6736(94)90067-1).

- (30) Calafiore, R. Microencapsulated Pancreatic Islet Allografts Into Nonimmunosuppressed Patients With Type 1 Diabetes: First Two Cases. *Diabetes Care* **2006**, *29* (1), 137–138.  
<https://doi.org/10.2337/diacare.29.1.137>.
- (31) Matsumoto, S.; Abalovich, A.; Wechsler, C.; Wynyard, S.; Elliott, R. B. Clinical Benefit of Islet Xenotransplantation for the Treatment of Type 1 Diabetes. *EBioMedicine* **2016**, *12*, 255–262.  
<https://doi.org/10.1016/j.ebiom.2016.08.034>.
- (32) Jacobs-Tulleneers-Thevissen, D.; Chintinne, M.; Ling, Z.; Gillard, P.; Schoonjans, L.; Delvaux, G.; Strand, B. L.; Gorus, F.; Keymeulen, B.; Pipeleers, D. Sustained Function of Alginate-Encapsulated Human Islet Cell Implants in the Peritoneal Cavity of Mice Leading to a Pilot Study in a Type 1 Diabetic Patient. *Diabetologia* **2013**, *56* (7), 1605–1614.  
<https://doi.org/10.1007/s00125-013-2906-0>.
- (33) Basta, G.; Montanucci, P.; Luca, G.; Boselli, C.; Noya, G.; Barbaro, B.; Qi, M.; Kinzer, K. P.; Oberholzer, J.; Calafiore, R. Long-Term Metabolic and Immunological Follow-up of Nonimmunosuppressed Patients with Type 1 Diabetes Treated with Microencapsulated Islet Allografts: Four Cases. *Diabetes Care* **2011**, *34* (11), 2406–2409. <https://doi.org/10.2337/dc11-0731>.
- (34) Tuch, B. E.; Keogh, G. W.; Williams, L. J.; Wu, W.; Foster, J. L.;

- Vaithilingam, V.; Philips, R. Safety and Viability of Microencapsulated Human Islets Transplanted into Diabetic Humans. *Diabetes Care* **2009**, *32* (10), 1887–1889. <https://doi.org/10.2337/dc09-0744>.
- (35) De Vos, P.; Spasojevic, M.; De Haan, B. J.; Faas, M. M. The Association between in Vivo Physicochemical Changes and Inflammatory Responses against Alginate Based Microcapsules. *Biomaterials* **2012**, *33* (22), 5552–5559. <https://doi.org/10.1016/j.biomaterials.2012.04.039>.
- (36) De Vos, P.; Van Hoogmoed, C. G.; De Haan, B. J.; Busscher, H. J. Tissue Responses against Immunoisolating Alginate-PLL Capsules in the Immediate Posttransplant Period. *J. Biomed. Mater. Res.* **2002**, *62* (3), 430–437. <https://doi.org/10.1002/jbm.10345>.
- (37) Bünger, C. M.; Gerlach, C.; Freier, T.; Schmitz, K. P.; Pilz, M.; Werner, C.; Jonas, L.; Schareck, W.; Hopt, U. T.; De Vos, P. Biocompatibility and Surface Structure of Chemically Modified Immunoisolating Alginate-PLL Capsules. *J. Biomed. Mater. Res. - Part A* **2003**, *67* (4), 1219–1227. <https://doi.org/10.1002/jbm.a.10094>.
- (38) Rokstad, A. M. A.; Lacík, I.; de Vos, P.; Strand, B. L. Advances in Biocompatibility and Physico-Chemical Characterization of Microspheres for Cell Encapsulation. *Advanced Drug Delivery Reviews*. Elsevier April 10, 2014, pp 111–130. <https://doi.org/10.1016/j.addr.2013.07.010>.
- (39) Anderson, J. M.; Rodriguez, A.; Chang, D. T. Foreign Body Reaction to

Biomaterials. *Seminars in Immunology*. Academic Press April 1, 2008, pp 86–100. <https://doi.org/10.1016/j.smim.2007.11.004>.

- (40) Williams, D. F. On the Mechanisms of Biocompatibility. *Biomaterials* **2008**, 29 (20), 2941–2953. <https://doi.org/10.1016/j.biomaterials.2008.04.023>.
- (41) Wilson, C. J.; Clegg, R. E.; Leavesley, D. I.; Pearcy, M. J. Mediation of Biomaterial-Cell Interactions by Adsorbed Proteins: A Review. *Tissue Engineering*. Mary Ann Liebert, Inc. 2 Madison Avenue Larchmont, NY 10538 USA January 28, 2005, pp 1–18. <https://doi.org/10.1089/ten.2005.11.1>.
- (42) Jenney, C. R.; Anderson, J. M. Adsorbed IgG: A Potent Adhesive Substrate for Human Macrophages. *J. Biomed. Mater. Res.* **2000**, 50 (3), 281–290. [https://doi.org/10.1002/\(SICI\)1097-4636\(20000605\)50:3<281::AID-JBM1>3.0.CO;2-5](https://doi.org/10.1002/(SICI)1097-4636(20000605)50:3<281::AID-JBM1>3.0.CO;2-5).
- (43) Jenney, C. R.; Anderson, J. M. Adsorbed Serum Proteins Responsible for Surface Dependent Human Macrophage Behavior. *J. Biomed. Mater. Res.* **2000**, 49 (4), 435–447. [https://doi.org/10.1002/\(SICI\)1097-4636\(20000315\)49:4<435::AID-JBM2>3.0.CO;2-Y](https://doi.org/10.1002/(SICI)1097-4636(20000315)49:4<435::AID-JBM2>3.0.CO;2-Y).
- (44) Vogler, E. A. Protein Adsorption in Three Dimensions. *Biomaterials* **2012**, 33 (5), 1201–1237. <https://doi.org/10.1016/j.biomaterials.2011.10.059>.
- (45) Chen, S.; Li, L.; Zhao, C.; Zheng, J. Surface Hydration: Principles and

Applications toward Low-Fouling/Nonfouling Biomaterials. *Polymer*.

Elsevier Ltd October 29, 2010, pp 5283–5293.

<https://doi.org/10.1016/j.polymer.2010.08.022>.

- (46) Leng, C.; Huang, H.; Zhang, K.; Hung, H.-C.; Xu, Y.; Li, Y.; Jiang, S.; Chen, Z. Effect of Surface Hydration on Antifouling Properties of Mixed Charged Polymers. *Langmuir* **2018**, *34* (22), 6538–6545.  
<https://doi.org/10.1021/acs.langmuir.8b00768>.
- (47) Chen, S.; Zheng, J.; Li, L.; Jiang, S. Strong Resistance of Phosphorylcholine Self-Assembled Monolayers to Protein Adsorption: Insights into Nonfouling Properties of Zwitterionic Materials. *J. Am. Chem. Soc.* **2005**, *127* (41), 14473–14478. <https://doi.org/10.1021/ja054169u>.
- (48) Laftah, W. A.; Hashim, S.; Ibrahim, A. N. Polymer Hydrogels: A Review. *Polym. Plast. Technol. Eng.* **2011**, *50* (14), 1475–1486.  
<https://doi.org/10.1080/03602559.2011.593082>.
- (49) Caló, E.; Khutoryanskiy, V. V. Biomedical Applications of Hydrogels: A Review of Patents and Commercial Products. *European Polymer Journal*. Elsevier Ltd April 1, 2015, pp 252–267.  
<https://doi.org/10.1016/j.eurpolymj.2014.11.024>.
- (50) Chai, Q.; Jiao, Y.; Yu, X. Hydrogels for Biomedical Applications: Their Characteristics and the Mechanisms behind Them. *Gels* **2017**, *3* (1), 6.  
<https://doi.org/10.3390/gels3010006>.

- (51) Tam, S. K.; de Haan, B. J.; Faas, M. M.; Hallé, J.-P.; Yahia, L.; de Vos, P. Adsorption of Human Immunoglobulin to Implantable Alginate-Poly-L-Lysine Microcapsules: Effect of Microcapsule Composition. *J. Biomed. Mater. Res. Part A* **2009**, *89A* (3), 609–615. <https://doi.org/10.1002/jbm.a.32002>.
- (52) Robitaille, R.; Dusseault, J.; Henley, N.; Desbiens, K.; Labrecque, N.; Hallé, J. P. Inflammatory Response to Peritoneal Implantation of Alginate-Poly-L-Lysine Microcapsules. *Biomaterials* **2005**, *26* (19), 4119–4127. <https://doi.org/10.1016/j.biomaterials.2004.10.028>.
- (53) de Vos, P.; van Hoogmoed, C. G.; de Haan, B. J.; Busscher, H. J. Tissue Responses against Immunoisolating Alginate-PLL Capsules in the Immediate Posttransplant Period. *J. Biomed. Mater. Res.* **2002**, *62* (3), 430–437. <https://doi.org/10.1002/jbm.10345>.
- (54) Daemi, H.; Barikani, M. Synthesis and Characterization of Calcium Alginate Nanoparticles, Sodium Homopolymannuronate Salt and Its Calcium Nanoparticles. *Sci. Iran.* **2012**, *19* (6), 2023–2028. <https://doi.org/10.1016/j.scient.2012.10.005>.
- (55) Grant, G. T.; Morris, E. R.; Rees, D. A.; Smith, P. J. C.; Thom, D. Biological Interactions between Polysaccharides and Divalent Cations: The Egg-Box Model. *FEBS Lett.* **1973**, *32* (1), 195–198. [https://doi.org/10.1016/0014-5793\(73\)80770-7](https://doi.org/10.1016/0014-5793(73)80770-7).



- (56) Martinsen, A.; Skjåk-Bræk, G.; Smidsrød, O. Alginate as Immobilization Material: I. Correlation between Chemical and Physical Properties of Alginate Gel Beads. *Biotechnol. Bioeng.* **1989**, *33* (1), 79–89.  
<https://doi.org/10.1002/bit.260330111>.
- (57) Kuo, C. K.; Ma, P. X. Ionically Crosslinked Alginate Hydrogels as Scaffolds for Tissue Engineering: Part 1. Structure, Gelation Rate and Mechanical Properties. *Biomaterials* **2001**, *22* (6), 511–521.  
[https://doi.org/10.1016/S0142-9612\(00\)00201-5](https://doi.org/10.1016/S0142-9612(00)00201-5).
- (58) Sikorski, P.; Mo, F.; Skjåk-Bræk, G.; Stokke, B. T. Evidence for Egg-Box-Compatible Interactions in Calcium - Alginate Gels from Fiber x-Ray Diffraction. *Biomacromolecules* **2007**, *8* (7), 2098–2103.  
<https://doi.org/10.1021/bm0701503>.
- (59) Chan, E. S.; Lim, T. K.; Voo, W. P.; Pogaku, R.; Tey, B. T.; Zhang, Z. Effect of Formulation of Alginate Beads on Their Mechanical Behavior and Stiffness. *Particuology* **2011**, *9* (3), 228–234.  
<https://doi.org/10.1016/j.partic.2010.12.002>.
- (60) Treml, H.; Woelki, S.; Kohler, H. H. Theory of Capillary Formation in Alginate Gels. *Chem. Phys.* **2003**, *293* (3), 341–353.  
[https://doi.org/10.1016/S0301-0104\(03\)00336-7](https://doi.org/10.1016/S0301-0104(03)00336-7).
- (61) Sonogo, J. M.; Santagapita, P. R.; Perullini, M.; Jobbágy, M. Ca(II) and Ce(III) Homogeneous Alginate Hydrogels from the Parent Alginic Acid

Precursor: A Structural Study. *Dalt. Trans.* **2016**, 45 (24), 10050–10057.

<https://doi.org/10.1039/c6dt00321d>.


- (62) Narayanan, R. P.; Melman, G.; Letourneau, N. J.; Mendelson, N. L.; Melman, A. Photodegradable Iron(III) Cross-Linked Alginate Gels. *Biomacromolecules* **2012**, 13 (8), 2465–2471.  
<https://doi.org/10.1021/bm300707a>.
- (63) Mørch, Y. A.; Qi, M.; Gundersen, P. O. M.; Formo, K.; Lacik, I.; Skjåk-Bræk, G.; Oberholzer, J.; Strand, B. L. Binding and Leakage of Barium in Alginate Microbeads. *J. Biomed. Mater. Res. - Part A* **2012**, 100 A (11), 2939–2947. <https://doi.org/10.1002/jbm.a.34237>.
- (64) Qi, M.; Strand, B. L.; Mørch, Y.; Lacík, I.; Wang, Y.; Salehi, P.; Barbaro, B.; Gangemi, A.; Kuechle, J.; Romagnoli, T.; et al. Encapsulation of Human Islets in Novel Inhomogeneous Alginate-Ca<sup>2+</sup>/Ba<sup>2+</sup> Microbeads: *In Vitro* and *In Vivo* Function. *Artif. Cells, Blood Substitutes, Biotechnol.* **2008**, 36 (5), 403–420. <https://doi.org/10.1080/10731190802369755>.
- (65) Ramos, P. E.; Silva, P.; Alario, M. M.; Pastrana, L. M.; Teixeira, J. A.; Cerqueira, M. A.; Vicente, A. A. Effect of Alginate Molecular Weight and M/G Ratio in Beads Properties Foreseeing the Protection of Probiotics. *Food Hydrocoll.* **2018**, 77, 8–16.  
<https://doi.org/10.1016/j.foodhyd.2017.08.031>.
- (66) de Haan, B. J.; Rossi, A.; Faas, M. M.; Smelt, M. J.; Sonvico, F.; Colombo,

- P.; de Vos, P. Structural Surface Changes and Inflammatory Responses against Alginate-Based Microcapsules after Exposure to Human Peritoneal Fluid. *J. Biomed. Mater. Res. Part A* **2011**, *98A* (3), 394–403.  
<https://doi.org/10.1002/jbm.a.33123>.
- (67) De Vos, P.; De Haan, B. J.; Wolters, G. H. J.; Strubbe, J. H.; Van Schilfgaarde, R. Improved Biocompatibility but Limited Graft Survival after Purification of Alginate for Microencapsulation of Pancreatic Islets. *Diabetologia* **1997**, *40* (3), 262–270.  
<https://doi.org/10.1007/s001250050673>.
- (68) Dusseault, J.; Tam, S. K.; Ménard, M.; Polizu, S.; Jourdan, G.; Yahia, L.; Hallé, J.-P. Evaluation of Alginate Purification Methods: Effect on Polyphenol, Endotoxin, and Protein Contamination. *J. Biomed. Mater. Res. Part A* **2006**, *76A* (2), 243–251. <https://doi.org/10.1002/jbm.a.30541>.
- (69) Mallett, A. G.; Korbitt, G. S. Alginate Modification Improves Long-Term Survival and Function of Transplanted Encapsulated Islets. *Tissue Eng. - Part A* **2009**, *15* (6), 1301–1309. <https://doi.org/10.1089/ten.tea.2008.0118>.
- (70) Paredes-Juarez, G. A.; De Haan, B. J.; Faas, M. M.; De Vos, P. The Role of Pathogen-Associated Molecular Patterns in Inflammatory Responses against Alginate Based Microcapsules. *J. Control. Release* **2013**, *172* (3), 983–992. <https://doi.org/10.1016/j.jconrel.2013.09.009>.
- (71) Lum, Z. P.; Krestow, M.; Tai, I. T.; Vacek, I.; Sun, A. M. Xenografts of Rat

Islets into Diabetic Mice an Evaluation of New Smaller Capsules.

*Transplantation* **1992**, 53 (6), 1180–1183.

<https://doi.org/10.1097/00007890-199206000-00002>.

- (72) Robitaille, R.; Pariseau, J.-F.; Leblond, F. A.; Lamoureux, M.; Lepage, Y.; Hall , J.-P. Studies on Small (<math>350 \mu\text{M}</math>) Alginate-Poly-L-Lysine Microcapsules. III. Biocompatibility of Smaller versus Standard Microcapsules. *J. Biomed. Mater. Res.* **1999**, 44 (1), 116–120.  
[https://doi.org/10.1002/\(SICI\)1097-4636\(199901\)44:1<116::AID-JBM13>3.0.CO;2-9](https://doi.org/10.1002/(SICI)1097-4636(199901)44:1<116::AID-JBM13>3.0.CO;2-9).
- (73) Veisoh, O.; Doloff, J. C.; Ma, M.; Vegas, A. J.; Tam, H. H.; Bader, A. R.; Li, J.; Langan, E.; Wyckoff, J.; Loo, W. S.; et al. Size- and Shape-Dependent Foreign Body Immune Response to Materials Implanted in Rodents and Non-Human Primates. *Nat. Mater.* **2015**, 14 (6), 643–651.  
<https://doi.org/10.1038/nmat4290>.
- (74) Bead Generators for Cell Encapsulation - DuPont Nutrition Norge AS  
<https://www.novamatrix.biz/bead-generators-for-cell-encapsulation/>  
(accessed May 19, 2020).
- (75) Bressel, T. A. B.; Paz, A. H.; Baldo, G.; Lima, E. O. C.; Matte, U.; Saraiva-Pereira, M. L. An Effective Device for Generating Alginate Microcapsules. *Genet. Mol. Biol.* **2008**, 31 (1), 136–140. <https://doi.org/10.1590/S1415-47572008000100023>.

- (76) Sugiura, S.; Oda, T.; Aoyagi, Y.; Matsuo, R.; Enomoto, T.; Matsumoto, K.; Nakamura, T.; Satake, M.; Ochiai, A.; Ohkohchi, N.; et al. Microfabricated Airflow Nozzle for Microencapsulation of Living Cells into 150 Micrometer Microcapsules. *Biomed. Microdevices* **2007**, *9* (1), 91–99.  
<https://doi.org/10.1007/s10544-006-9011-9>.
- (77) Skjåk-Bræk, G.; Grasdalen, H.; Smidsrød, O. Inhomogeneous Polysaccharide Ionic Gels. *Carbohydr. Polym.* **1989**, *10* (1), 31–54.  
[https://doi.org/10.1016/0144-8617\(89\)90030-1](https://doi.org/10.1016/0144-8617(89)90030-1).
- (78) De Vos, P.; De Haan, B. J.; Van Schilfgaarde, R. Upscaling the Production of Microencapsulated Pancreatic Islets. *Biomaterials* **1997**, *18* (16), 1085–1090. [https://doi.org/10.1016/S0142-9612\(97\)00040-9](https://doi.org/10.1016/S0142-9612(97)00040-9).
- (79) Hallé, J. P.; Bourassa, S.; Leblond, F. A.; Chevalier, S.; Beaudry, M.; Chapdelaine, A.; Cousineau, S.; Saintonoe, J.; Yale, J. F. Protection of Islets of Langerhans from Antibodies by Microencapsulation with Alginate-Poly-L-Lysine Membranes. *Transplantation* **1993**, *55* (2), 350–354.  
<https://doi.org/10.1097/00007890-199302000-00023>.
- (80) Wolters, G. H. J.; Fritschy, W. M.; Gerrits, D.; Van Schilfgaarde, R. A Versatile Alginate Droplet Generator Applicable for Microencapsulation of Pancreatic Islets. *J. Appl. Biomater.* **1992**, *3* (4), 281–286.  
<https://doi.org/10.1002/jab.770030407>.
- (81) Klokk, T. I.; Melvik, J. E. Controlling the Size of Alginate Gel Beads by Use

of a High Electrostatic Potential. *J. Microencapsul.* **2002**, 19 (4), 415–424.  
<https://doi.org/10.1080/02652040210144234>.

- (82) Poncelet, D.; Neufeld, R. J.; Goosen, M. F. A.; Burgarski, B.; Babak, V.  
Formation of Microgel Beads by Electric Dispersion of Polymer Solutions.  
*AIChE J.* **1999**, 45 (9), 2018–2023. <https://doi.org/10.1002/aic.690450918>.
- (83) Lewińska, D.; Rosiński, S.; Weryński, A. Influence of Process Conditions  
During Impulsed Electrostatic Droplet Formation on Size Distribution of  
Hydrogel Beads. *Artif. Cells, Blood Substitutes, Biotechnol.* **2004**, 32 (1),  
41–53. <https://doi.org/10.1081/BIO-120028667>.
- (84) Shintaku, H.; Kuwabara, T.; Kawano, S.; Suzuki, T.; Kanno, I.; Kotera, H.  
Micro Cell Encapsulation and Its Hydrogel-Beads Production Using  
Microfluidic Device. In *Microsystem Technologies*; Springer, 2007; Vol. 13,  
pp 951–958. <https://doi.org/10.1007/s00542-006-0291-z>.
- (85) Choi, C. H.; Jung, J. H.; Rhee, Y. W.; Kim, D. P.; Shim, S. E.; Lee, C. S.  
Generation of Monodisperse Alginate Microbeads and in Situ  
Encapsulation of Cell in Microfluidic Device. *Biomed. Microdevices* **2007**, 9  
(6), 855–862. <https://doi.org/10.1007/s10544-007-9098-7>.
- (86) Tan, W.-H.; Takeuchi, S. Monodisperse Alginate Hydrogel Microbeads for  
Cell Encapsulation. *Adv. Mater.* **2007**, 19 (18), 2696–2701.  
<https://doi.org/10.1002/adma.200700433>.

- (87) Rossow, T.; Heyman, J. A.; Ehrlicher, A. J.; Langhoff, A.; Weitz, D. A.; Haag, R.; Seiffert, S. Controlled Synthesis of Cell-Laden Microgels by Radical-Free Gelation in Droplet Microfluidics. *J. Am. Chem. Soc.* **2012**, *134* (10), 4983–4989. <https://doi.org/10.1021/ja300460p>.
- (88) Akbari, S.; Pirbodaghi, T. Microfluidic Encapsulation of Cells in Alginate Particles via an Improved Internal Gelation Approach. *Microfluid. Nanofluidics* **2014**, *16* (4), 773–777. <https://doi.org/10.1007/s10404-013-1264-z>.
- (89) Johnson, M. A.; Kleinberger, R.; Abu Helal, A.; Latchminarine, N.; Ayyash, A.; Shi, S.; Burke, N. A. D.; Holloway, A. C.; Stöver, H. D. H. Quantifying Cellular Protrusion in Alginate Capsules with Covalently Crosslinked Shells. *J. Microencapsul.* **2019**, *36* (5), 421–431. <https://doi.org/10.1080/02652048.2019.1618404>.
- (90) Bhujbal, S. V.; de Haan, B.; Niclou, S. P.; de Vos, P. A Novel Multilayer Immunoisolating Encapsulation System Overcoming Protrusion of Cells. *Sci. Rep.* **2014**, *4*, 6856. <https://doi.org/10.1038/srep06856>.
- (91) Ma, M.; Chiu, A.; Sahay, G.; Doloff, J. C.; Dholakia, N.; Thakrar, R.; Cohen, J.; Vegas, A.; Chen, D.; Bratlie, K. M.; et al. Core-Shell Hydrogel Microcapsules for Improved Islets Encapsulation. *Adv. Healthc. Mater.* **2013**, *2* (5), 667–672. <https://doi.org/10.1002/adhm.201200341>.
- (92) Lienemann, P. S.; Rossow, T.; Mao, A. S.; Vallmajo-Martin, Q.; Ehrbar, M.;

Mooney, D. J. Single Cell-Laden Protease-Sensitive Microniches for Long-Term Culture in 3D. *Lab Chip* **2017**, *17* (4), 727–737.

<https://doi.org/10.1039/C6LC01444E>.

- (93) Kamperman, T.; Henke, S.; Visser, C. W.; Karperien, M.; Leijten, J. Centering Single Cells in Microgels via Delayed Crosslinking Supports Long-Term 3D Culture by Preventing Cell Escape. *Small* **2017**, *13* (22), 1603711. <https://doi.org/10.1002/smll.201603711>.
- (94) Strand, B. L.; Mørch, Y. A.; Espevik, T.; Skjåk-Braek, G. Visualization of Alginate-Poly-L-Lysine-Alginate Microcapsules by Confocal Laser Scanning Microscopy. *Biotechnol. Bioeng.* **2003**, *82* (4), 386–394. <https://doi.org/10.1002/bit.10577>.
- (95) Simó, G.; Fernández-Fernández, E.; Vila-Crespo, J.; Ruipérez, V.; Rodríguez-Nogales, J. M. Research Progress in Coating Techniques of Alginate Gel Polymer for Cell Encapsulation. *Carbohydrate Polymers*. Elsevier Ltd August 15, 2017, pp 1–14. <https://doi.org/10.1016/j.carbpol.2017.04.013>.
- (96) Fischer, D.; Li, Y.; Ahlemeyer, B.; Krieglstein, J.; Kissel, T. In Vitro Cytotoxicity Testing of Polycations: Influence of Polymer Structure on Cell Viability and Hemolysis. *Biomaterials* **2003**, *24* (7), 1121–1131. [https://doi.org/10.1016/S0142-9612\(02\)00445-3](https://doi.org/10.1016/S0142-9612(02)00445-3).
- (97) Monnery, B. D.; Wright, M.; Cavill, R.; Hoogenboom, R.; Shaunak, S.;



Steinke, J. H. G.; Thanou, M. Cytotoxicity of Polycations: Relationship of Molecular Weight and the Hydrolytic Theory of the Mechanism of Toxicity. *Int. J. Pharm.* **2017**, *521* (1–2), 249–258.  
<https://doi.org/10.1016/j.ijpharm.2017.02.048>.

- (98) Rokstad, A. M.; Brekke, O.-L.; Steinkjer, B.; Ryan, L.; Kolláriková, G.; Strand, B. L.; Skjåk-Bræk, G.; Lambris, J. D.; Lacík, I.; Mollnes, T. E.; et al. The Induction of Cytokines by Polycation Containing Microspheres by a Complement Dependent Mechanism. *Biomaterials* **2013**, *34* (3), 621–630.  
<https://doi.org/10.1016/j.biomaterials.2012.10.012>.
- (99) Bünger, C. M.; Gerlach, C.; Freier, T.; Schmitz, K. P.; Pilz, M.; Werner, C.; Jonas, L.; Schareck, W.; Hopt, U. T.; De Vos, P. Biocompatibility and Surface Structure of Chemically Modified Immunoisolating Alginate-PLL Capsules. *J. Biomed. Mater. Res. - Part A* **2003**, *67* (4), 1219–1227.  
<https://doi.org/10.1002/jbm.a.10094>.
- (100) Wei, Q.; Becherer, T.; Angioletti-Uberti, S.; Dzubiella, J.; Wischke, C.; Neffe, A. T.; Lendlein, A.; Ballauff, M.; Haag, R. Protein Interactions with Polymer Coatings and Biomaterials. *Angew. Chemie Int. Ed.* **2014**, *53* (31), 8004–8031. <https://doi.org/10.1002/anie.201400546>.
- (101) Tam, S. K.; Bilodeau, S.; Dusseault, J.; Langlois, G.; Hallé, J. P.; Yahia, L. H. Biocompatibility and Physicochemical Characteristics of Alginate-Polycation Microcapsules. *Acta Biomater.* **2011**, *7* (4), 1683–1692.

<https://doi.org/10.1016/j.actbio.2010.12.006>.

- (102) Spasojevic, M.; Paredes-Juarez, G. A.; Vorenkamp, J.; de Haan, B. J.; Schouten, A. J.; de Vos, P. Reduction of the Inflammatory Responses against Alginate-Poly-L-Lysine Microcapsules by Anti-Biofouling Surfaces of PEG-b-PLL Diblock Copolymers. *PLoS One* **2014**, *9* (10), e109837. <https://doi.org/10.1371/journal.pone.0109837>.
- (103) Sawhney, A. S.; Hubbell, J. A. Poly(Ethylene Oxide)-Graft-Poly(L-Lysine) Copolymers to Enhance the Biocompatibility of Poly(L-Lysine)-Alginate Microcapsule Membranes. *Biomaterials* **1992**, *13* (12), 863–870. [https://doi.org/10.1016/0142-9612\(92\)90180-V](https://doi.org/10.1016/0142-9612(92)90180-V).
- (104) Abu Lila, A. S.; Shimizu, T.; Ishida, T. PEGylation and Anti-PEG Antibodies. In *Engineering of Biomaterials for Drug Delivery Systems: Beyond Polyethylene Glycol*; Elsevier Inc., 2018; pp 51–68. <https://doi.org/10.1016/B978-0-08-101750-0.00003-9>.
- (105) Kleinberger, R. M.; Burke, N. A. D.; Zhou, C.; Stover, H. D. H. Synthetic Polycations with Controlled Charge Density and Molecular Weight as Building Blocks for Biomaterials. *J. Biomater. Sci. Polym. Ed.* **2016**, *27* (4), 351–369. <https://doi.org/10.1080/09205063.2015.1130407>.
- (106) Hastings, D. E.; Stöver, H. D. H. Crosslinked Hydrogel Capsules for Cell Encapsulation Formed Using Amino/Betaine Dual-Functional Semibatch Copolymers. *ACS Appl. Polym. Mater.* **2019**, *1* (8), 2055–2067.

<https://doi.org/10.1021/acsapm.9b00124>.

- (107) Ros, S.; Burke, N. A. D.; Stöver, H. D. H. Synthesis and Properties of Charge-Shifting Polycations: Poly[3-Aminopropylmethacrylamide- Co -2-(Dimethylamino)Ethyl Acrylate]. *Macromolecules* **2015**, *48* (24), 8958–8970. <https://doi.org/10.1021/acs.macromol.5b02191>.
- (108) Rokstad, A. M.; Holtan, S.; Strand, B.; Steinkjer, B.; Ryan, L.; Kulseng, B.; Skjåk-Bræk, G.; Espevik, T. Microencapsulation of Cells Producing Therapeutic Proteins: Optimizing Cell Growth and Secretion. *Cell Transplant.* **2002**, *11* (4), 313–324.  
<https://doi.org/10.3727/000000002783985774>.
- (109) Gardner, C. M.; Burke, N. A. D.; Stöver, H. D. H. Cross-Linked Microcapsules Formed From Self-Deactivating Reactive Polyelectrolytes. *Langmuir* **2010**, *26* (7), 4916–4924. <https://doi.org/10.1021/la903540c>.
- (110) Gardner, C. M.; Stöver, H. D. H. Reactive Polyanions Based on Poly(4,4-Dimethyl-2-Vinyl-2-Oxazoline-5-One- Co-Methacrylic Acid). *Macromolecules* **2011**, *44* (18), 7115–7123.  
<https://doi.org/10.1021/ma201409t>.
- (111) Jafar Mazumder, M. A.; Shen, F.; Burke, N. A. D.; Potter, M. A.; Stöver, H. D. H. Self-Cross-Linking Polyelectrolyte Complexes for Therapeutic Cell Encapsulation. *Biomacromolecules* **2008**, *9* (9), 2292–2300.  
<https://doi.org/10.1021/bm800580c>.

- (112) Gardner, C. M.; Burke, N. A. D.; Chu, T.; Shen, F.; Potter, M. A.; Stöver, H. D. H. Poly(Methyl Vinyl Ether-Alt-Maleic Acid) Polymers for Cell Encapsulation. *J. Biomater. Sci. Polym. Ed.* **2011**, *22* (16), 2127–2145. <https://doi.org/10.1163/092050610X535149>.
- (113) Gardner, C. M.; Potter, M. A.; Stöver, H. D. H. Improving Covalent Cell Encapsulation with Temporarily Reactive Polyelectrolytes. *J. Mater. Sci. Mater. Med.* **2012**, *23* (1), 181–193. <https://doi.org/10.1007/s10856-011-4523-0>.
- (114) Mahou, R.; Tran, N. M.; Dufresne, M.; Legallais, C.; Wandrey, C. Encapsulation of Huh-7 Cells within Alginate-Poly(Ethylene Glycol) Hybrid Microspheres. *J. Mater. Sci. Mater. Med.* **2012**, *23* (1), 171–179. <https://doi.org/10.1007/s10856-011-4512-3>.
- (115) Mahou, R.; Wandrey, C. Alginate–Poly(Ethylene Glycol) Hybrid Microspheres with Adjustable Physical Properties. *Macromolecules* **2010**, *43* (3), 1371–1378. <https://doi.org/10.1021/ma902469f>.
- (116) Mazumder, M. A. J.; Burke, N. A. D.; Shen, F.; Potter, M. A.; Stöver, H. D. H. Core-Cross-Linked Alginate Microcapsules for Cell Encapsulation. *Biomacromolecules* **2009**, *10* (6), 1365–1373. <https://doi.org/10.1021/bm801330j>.
- (117) Desai, N. P.; Sojomihardjo, A.; Yao, Z.; Ron, N.; Soon-Shiong, P. Interpenetrating Polymer Networks of Alginate and Polyethylene Glycol for

Encapsulation of Islets of Langerhans. *J. Microencapsul.* **2000**, 17 (6), 677–690. <https://doi.org/10.1080/02652040050161675>.

- (118) Meier, R. P. H.; Mahou, R.; Morel, P.; Meyer, J.; Montanari, E.; Muller, Y. D.; Christofilopoulos, P.; Wandrey, C.; Gonelle-Gispert, C.; Bühler, L. H. Microencapsulated Human Mesenchymal Stem Cells Decrease Liver Fibrosis in Mice. *J. Hepatol.* **2015**, 62 (3), 634–641. <https://doi.org/10.1016/j.jhep.2014.10.030>.

## **Chapter 2 - Quantifying Cellular Protrusion in Alginate Capsules with Covalently Crosslinked Shells**

Mitchell A. Johnson<sup>a</sup>, Rachele Kleinberger<sup>a</sup>, Ali Abu Helal<sup>b</sup>, Nicole Latchminarine<sup>b</sup>, Ahmed Ayyash<sup>b</sup>, Shanna Shi<sup>a</sup>, Nicholas A.D. Burke<sup>a</sup>, Alison C. Holloway<sup>b</sup>, Harald D.H. Stöver<sup>a\*</sup>

<sup>a</sup>*Dept. of Chemistry and Chemical Biology, McMaster University, Hamilton, ON, Canada;* <sup>b</sup>*Dept. of Obstetrics and Gynecology, McMaster University, Hamilton, ON, Canada.*

### **2.1 Abstract**

This work describes viability and distribution of INS-1E beta cells in shell-crosslinked alginate capsules, focussing on cells located near the capsule surface. Capsules were formed by air-shearing alginate suspensions of INS-1E cells into a gelling bath, and coating with poly-L-lysine (PLL) and 50% hydrolyzed poly(methylvinylether-alt-maleic anhydride) to form crosslinked networks reinforcing the capsule surfaces. The percentage of cells at the capsule surface were determined using 2D and 3D confocal colocalization mapping. Encapsulated INS-1E cells showed high cell viability and progressive cell clustering out to six weeks. About 30% of cells were initially colocated with the 20 micrometer thick alginate-PLL-PMM50 shell, with 7% of cells protruded at the capsule surfaces, both reflecting random cell distributions. Protruding cells may cause cell-based immune responses, weaken capsules, and potentially result in cell escape from the capsules. The data shown indicate that

reinforcing capsules with crosslinked shells may assist in preventing cell exposure and escape.

## **2.2 Introduction**

Chronic endocrine disorders such as diabetes are increasing at a staggering pace, with insulin-dependent forms of diabetes affecting about 1 % of the adult population.<sup>1</sup> The current standard of care guidelines issued by the American Diabetes Association for insulin-dependent diabetes involves multiple daily injections of insulin or continuous insulin infusion<sup>1,2</sup> but neither of these can completely avoid long term pathologies due to poor blood sugar regulation. In contrast, cell-based insulin replacement therapies aim to use transplanted cells to release insulin as needed, using biofeedback to maintain blood glucose levels. Transplantation of donor-derived pancreatic islets according to the Edmonton Protocol<sup>3,4</sup> has shown insulin independence in about 50% of recipients for at least five years but requires lifelong immuno-suppression.

Lim and Sun<sup>5</sup> demonstrated that pancreatic islets encapsulated in calcium alginate hydrogel capsules could cure diabetes in allogenic rat models for at least several weeks. Encapsulating cells should offer physical immune-protection from the host's immune system, without need for ongoing immune suppression.<sup>6</sup> Even autologous insulin producing cells would benefit from this approach as type 1 diabetes (T1D) is an auto-immune disorder that can attack any cells producing insulin.<sup>7</sup>

To date, such capsules often still develop fibrotic overgrowth, that is only partially resolved by coating the capsules with heparin<sup>8</sup> or PEG derivatives.<sup>9</sup> These immune responses are attributed i.a. to polycation coatings<sup>10</sup>, residual biological impurities present in alginate<sup>11</sup>, and immune markers inherent in alginate.<sup>12</sup>

Several approaches have been developed to mitigate surface-triggered immune responses to cell-containing capsules. Re-engineering alginate as well as adding anti-fouling crosslinked shells seem particularly promising in that regard.<sup>13,14</sup> Our lab showed previously that 50% hydrolyzed poly(methylvinylether-alt-maleic anhydride), PMM50, can be deposited on poly-L-lysine-coated alginate capsules to form a crosslinked PLL-PMM50 polyampholyte network within the outer 20 micrometer of calcium alginate capsules. These capsules protected C2C12 cells during peritoneal implantation in immunocompetent C57BL/6 mice for six weeks; mice implanted with PMM50 coated capsules had significantly lower levels of serum inflammatory markers and reduced capsular fibrosis, compared to alginate - PLL - alginate (APA) controls.<sup>15</sup>

A key remaining concern in cell encapsulation is the common observation of a small fraction of cells ending up near the surface of the capsule, or even protruding from it. Such cells can attract an immediate contact-mediated immune response from the host that could be responsible for some of the residual immune response observed in the previous work.<sup>15</sup> Worse, protruding cells could



potentially escape to form teratomas.<sup>16,17</sup> Dusseault et al. previously showed that crosslinked shells can contain aggressively expanding cancer cells within the capsules<sup>16</sup>, but this does not address concerns about cells protruding from the actual, crosslinked shell in the first place. For single cell capsules produced by water/oil microfluidic processes, microfluidic centering with delayed gelation or by agitation with orbital shaking during gelation have been shown to allow single cells to be positioned and immobilized in central positions within ca 20 micrometer gel beads.<sup>18,19</sup> Water-in-oil emulsion processes using higher alginate concentrations<sup>6</sup> have shown fewer cells near the capsule surface.<sup>20,21</sup> For conventional, 200 - 500 micrometer alginate capsules formed by air or electrostatic shearing into an aqueous calcium chloride gelling bath, several groups have addressed cell protrusion by adding an outer gel layer to cell-containing core capsules, though this comes at the cost of an order of magnitude increase in dead volume, which negatively impacts fill factor and diffusional rates.<sup>22-24</sup> New methods to measure and ultimately mitigate cell protrusion from such large alginate-type capsules will have to be developed.

The current paper describes the encapsulation of pancreatic INS-1E cells in calcium alginate capsules that were then coated with crosslinked PLL-PMM50 polymer shells using a method described previously.<sup>15</sup> It describes viability and behaviour of this insulinoma cell line within these shell-crosslinked, antifouling capsules. In addition, it describes fluorescence microscopy methods developed to quantify the fraction of encapsulated cells located at or near the capsule

surface, as illustrated in Scheme 1. These techniques should prove useful in assessing this key issue in current capsule technologies and may be used as quantitative tools in future work aimed at mitigating the problem of protruding cells.

## **2.3 Experimental**

### **2.3.1 Materials**

Poly(methylvinylether-alt-maleic anhydride) (MW 80kDa, Sigma Aldrich) was heated under vacuum for 96 hrs at 110°C to ensure any hydrolyzed anhydride units are dehydrated back to the anhydride form. Poly-L-lysine HBr (15 - 30 kDa) was obtained from Polysciences. UP-MVG sodium alginate BP-1603-09 was obtained from FMC Biosciences. Deuterated acetonitrile 99.96% D was obtained from Cambridge Isotope Laboratories. Fluorescent LIVE/DEAD assay kits based on Calcein AM/Ethidium homodimer and 20mM Hoechst 3342 was obtained from Thermo Fisher Scientific. Deuterium dioxide 99.9 % D, Rhodamine isothiocyanate (RITC), Trypan blue stain 0.4%, Phosphate buffered saline, Trypsin EDTA 0.25%, HEPES sodium salt, RPMI-1640, HEPES 1M, 100mM Sodium Pyruvate, 55mM  $\beta$ -mercaptoethanol, 200mM Glutamine, fetal bovine serum, Gibco, heat-inactivated at 56°C for 30 min prior to use, Dextran-FITC 2000 kDa were purchased from (Sigma Aldrich, Oakville, ON). All reagents and chemicals were used as received. Calcium Chloride dihydrate and Sodium

Chloride were purchased from (Caledon Laboratories Ltd, ON), Sodium Hydroxide was purchased from Labchem INC, (Tri)sodium citrate dihydrate was purchased from EMD chemicals. All reagents and chemicals were used as received.

### **2.3.2 Synthesis of 50% hydrolyzed poly(methylvinylether-alt-maleic anhydride), PMM<sub>50</sub>**

PMM<sub>50</sub> was prepared by a method adapted from one previously described by our group.<sup>15</sup> Commercial poly(methylvinylether-alt-maleic anhydride), PMM, in anhydride form was heated under vacuum at 110°C for 96 hours in order to convert any trace of succinic acid groups back to the anhydride form. Subsequently, 50.3 mg of this PMM was dissolved in 450uL of deuterated acetonitrile in an 8 mL screw cap glass vial. 50uL of deuterated water was added to form a 9:1 acetonitrile:water ratio, and the vial heated at 55°C for 18 hrs. 1H-NMR spectra were acquired on a Bruker Avance 600 NMR spectrometer, and the progress of anhydride hydrolysis tracked by following the appearance of the succinic acid signals at 3.0 ppm, and the appearance and down field movement of the sharp peak representing total mobile protons. Hydrolysis was stopped completely after 18 hrs by cooling the reaction mixture to 4°C.

### **2.3.3 Cell Maintenance**

INS-1E cells, a rat insulinoma cell line, were generously provided by Dr.

Claes Wollheim (University of Geneva, Switzerland). Cells between passages 60-90 were cultured at 37°C in a humidified atmosphere of 95% O<sub>2</sub> and 5% CO<sub>2</sub>. Cells were grown in T75 tissue-culture treated flasks (Corning, 353003, Corning, NY, USA) in RPMI-1640 media supplemented with 1mM sodium pyruvate, 50µM β-mercaptoethanol, 1mM glutamine, 25 mM HEPES and 10% heat-inactivated fetal bovine serum.

### **2.3.4 Formation of Calcium Alginate Capsules**

INS-1E cell containing capsules were prepared by combining equal volumes (typically 2 mL) of INS-1E cells resuspended at a concentration of 4 million cells/mL in 0.22µm sterile filtered pH 7.4 HEPES-buffered saline solution, and of 0.22µm sterile filtered, 2% w/v UP-MVG Na-alginate in pH 7.4 HEPES buffered saline, in a sterile 50 mL Falcon tube. The tube was then manually agitated in the biosafety hood, with occasional immersion in an ice bath, for six minutes to form a homogeneous suspension of cells (2 million cells/mL) in 1% w/v Na-alginate. This suspension was taken up into a 10 mL BD plastic syringe fitted with a 16g bevelled tip needle, to minimize cell damage. The 16g needle was then replaced by a 27g blunt tipped needle, the syringe attached to a Harvard Apparatus Pump 11 Elite syringe pump fitted with an air-shearing adaptor and the suspension extruded at 8mL/hr liquid flow rate, with HEPA filtered concentric air flow at 2.5L/min, into 50 mL of 1.1% w/v CaCl<sub>2</sub> 0.45% w/v NaCl gelling bath in a 100 mL beaker with a 4.6cm inner diameter kept in an

external ice bath. The distance between needle tip and surface of gelling bath was 3.8cm. The capsules were allowed to gel for approximately an additional 5 minutes after completion of the extrusion. The same procedure was followed for cell-free model capsules, except that the 2% w/v MVG Na-alginate solution was diluted with an equal volume of pH 7.4 HEPES-buffered saline.

### **2.3.5 Formation of PLL / PMM<sub>50</sub> Crosslinked Shell**

The resulting cell-containing Ca-alginate capsules were transferred into a 50 mL Falcon tube and allowed to settle by gravity. The supernatant was removed and 0.3 mL aliquots of the resulting 3 mL of sedimented capsules were each resuspended in 1.5mL Eppendorff tubes in 1 mL fresh gelling bath. The tubes were inverted three time, the capsules allowed to settle by gravity, the supernatant was removed, and the capsules were then coated by adding 1 mL of 0.22µm sterile filtered 0.1% w/v PLL and agitating continuously by manual inversion for 6 minutes. The PLL-coated capsules were then washed twice with 1 mL 0.22µm sterile filtered saline, involving three manual inversions and sedimentation. The capsules were resuspended in 0.5 mL of 0.22µm sterile filtered pH 7.8 35mM HEPES-buffered saline. Separately, 0.1 mL of PMM<sub>50</sub> in 90:10 deuterated acetonitrile:deuterated water was added to 2.4mL of pH 7.4 35mM HEPES-buffered saline in an 8 mL glass vial, and the mixture vortexed for 15 seconds. Immediately after, 500µL of this solution was filtered through a 0.22µm filter directly into the Ca-alginate capsules suspension, followed by

mixing using manual inversion for 6 minutes. The PMM<sub>50</sub> coated Ca-alginate capsules were then allowed to sediment, washed once each with saline and with cell culture media in 3:10 volume and resuspended in RPMI cell culture media, and transferred into an interior well of a 24 well plate. Saline was placed into each of the surrounding wells in order to minimize evaporation for the bead suspensions. The plates were then transferred to a 37C 5% CO<sub>2</sub> mammalian cell culture incubator and the media was changed every two days.

### **2.3.6 Measuring Cell Viability using LIVE/DEAD Fluorescence Assay**

Cell viabilities were determined using fluorescent live/dead staining of cells with Calcein-AM and ethidium homodimer, and imaging with a Nikon A1R confocal microscope. For the staining procedure, an aliquot of cell-containing capsules was formed by depositing 1 to 2 droplets using a sterile transfer pipette into each well of a 96 well CellVis glass bottom plate. The cells were stained with 50 $\mu$ L of 10 $\mu$ M Calcein AM in pH 7.4 35mM HEPES-buffered saline and with 50 $\mu$ L of 3 $\mu$ M Ethidium Homodimer in pH 7.4 35mM HEPES-buffered saline. The cells were incubated with the staining solutions for 30 minutes at room temperature and then full 3D z-stacks of capsules were acquired. The ratio of live to dead cells was determined by averaging the number of live and dead stained cells from three capsules.

### **2.3.7 Testing Resistance of Crosslinked Shells to Citrate and NaOH**

To test for the covalent crosslinking of the PLL-PMM<sub>50</sub> shell, a drop of capsule suspension was placed on a microscope slide mounted on an inverted microscope. The supernatant was blotted away and immediately replaced with 1M Na-Citrate to chelate Ca<sup>2+</sup> ions and dissolve the Ca-alginate matrix. Subsequently, the supernatant was replaced with 0.1M NaOH and the capsules were lightly agitated. The treated capsules were then imaged on a Nikon Inverted microscope to assess for presence of a covalently crosslinked shell.

### **2.3.8 Synthesis of Rhodamine-labelled Poly-L-Lysine, PLLr**

PLLr was prepared as described previously.<sup>25</sup> Briefly, poly-L-lysine HBr (100 mg, 15-30 kDa) was dissolved in 10 mL of pH 9 0.2M NaHCO<sub>3</sub> buffer. Rhodamine Isothiocyanate (RITC, 5 mg) was dissolved in 1.92mL of DMF to make a 2.6mg/ml stock solution. 0.5mL of this RITC stock solution was added dropwise to the PLL solution under vigorous stirring and the mixture was allowed to react covered from light for 1hr at room temperature. The solution was then adjusted to pH 7 by addition of 1M HCl and placed in dialysis tubing (3.5 KDa cutoff) and exchanged against distilled water for three days with daily exchanges of water. The final solutions were freeze dried.

### **2.3.9 Confocal Fluorescence Colocalization of INS-1E Cells and Rhodamine-labelled (PLLr) Shells**

Cell-containing A-PLL-PM<sub>50</sub> capsules prepared as above but using rhodamine-labelled PLL (PLLr) to define the outer shells, were added to wells in a 96-well CellVis glass bottom plate to form a capsule monolayer. The cells were stained for 30 minutes with 50µL of 10µM Calcein AM solution. Z-stacks comprising 100 sections were obtained of multiple capsules. The average PLLr shell thickness and capsule diameter were measured manually as an average of 100 capsules with Nikon NIS Elements Advanced Research software.

Fractions of cells partially and fully colocalized within the PLLr shell were determined using ImageJ.fiji<sup>26</sup> and Nikon NIS Software. The PLLr and Calcein AM channels of the acquired z-stacks were thresholded separately in Nikon NIS to form binary images. For thresholding of the PLLr shell, a thresholding range was chosen that gave complete overlap of the binary mask with the PLLr fluorescent signal throughout the z-series. The thresholding range for the fluorescently stained cells was chosen such that there was complete overlap of the binary mask with the cells at their widest point in the z-stack. These binary images were then segmented into objects in ImageJ.fiji using 3D Simple Segmentation<sup>27</sup> to produce the corresponding 3D binary image stacks of shell and PLLr cells, respectively. Object to object distances between cell and PLLr shells were measured automatically using the ImageJ plugin Distance Analysis (DiAna).<sup>28</sup> Fractions of cells protruding beyond the PLLr-labelled shells were



determined by manually counting the number of protruding as well as internal cells in each Z-section, in Nikon NIS.

### **2.3.10 Confocal Fluorescence Colocalization of INS-1E Cells with Dextran-f containing continuous media**

AP-PMM<sub>50</sub> capsules formed using unlabelled PLL were placed as a sparse layer in several wells of a 96 well plate to allow for imaging of individual capsules per field of view in several wells of a 96 well plate. The cells in each well were stained with 100µl of 10µm Calcein-AM prepared in a 0.1% w/v 2 MDa dextran-f solution in pH 7.4 HEPES buffered saline for 30min. Confocal z-stacks of 100 sections were obtained for multiple capsules and channels. Prior to quantification of cellular protrusion, the axial scale was rescaled by a scaling factor calculated by the ratio of the equatorial diameter with the axial diameter defined by the top and bottom of the Z-stack. Before rescaling the original data show the capsule as ellipsoid. This is a common artifact in confocal imaging of thick samples and is due to the differences in refractive indices between air objective lens and the water refractive index, resulting in axial shrinking of the 3D rendered image.<sup>29</sup> This geometrical distortion will not affect the quantification of protruding or non-protruding cells but may affect the accuracy of distance to distance measurements in 3D. Axial shrinkage can be corrected by imaging with a water immersion objective lens to match the refractive index of the sample or by rescaling the Z-axis by applying a scaling factor. Protruding cells were

quantified by producing binary images of the cells and of the one-pixel wide outer edge of the capsule. The binary 3D image of the outer capsule edge was produced by first thresholding the low intensity pixels corresponding to the size exclusion of the 2MDa dextran-f at the capsule surface in the FITC channel. A thresholding range was chosen that gave overlap of the binary mask with the region of size exclusion of 2mDa dextran-f. After thresholding, edge detection and convex hull filtering were applied. A second thresholding of the FITC channel at higher intensities allowed identification of the Calcein-AM stained live cells without interference from the dextran-f. The resulting binary images were then automatically segmented into objects and then measured for the object-to-object distances between cells and capsule outer edge, as described above.

### **2.3.11 Statistical Analysis**

Cell viabilities and cellular protrusion measured by colocalization with dextran-f are expressed as the mean  $\pm$  SD of a triplicate of three cell encapsulation experiments. A single factor ANOVA was used assuming all means were equal. A P-value of  $< 0.05$  was used to determine statistically significant differences between means

## **2.4 Results**

### 2.4.1 Capsule Formation and Properties

Air-shearing cell suspensions in sodium alginate solutions into a calcium chloride gelling bath is a common approach to forming spherical cell-containing calcium alginate capsules of 200 - 1000 micrometer diameter.<sup>30</sup> Canaple showed that smaller capsules result in better performance of encapsulated cells, as their larger surface area to volume ratio improves oxygen and nutrient mass transport,<sup>31</sup> while Anderson and Langer showed better cell viability for 1500 micrometer than for 500 micron capsules.<sup>32</sup> Decreasing the bead diameter can certainly increase both the risk of cellular protrusion, at least for whole Islets<sup>33</sup>, and the risk of bead collapse during coating with PLL.<sup>34</sup>

For the current study we prepared capsules of about 500 micrometer diameters, arguably the most common size. We used a vertical syringe holder machined from a block of graphite-loaded Delrin (Appendix Figure 2.1), designed to accommodate a syringe equipped with needle gauges above 20 with a coaxial air flow. A series of experiments were carried out to examine the effects of annular airspeed on both bead size and on bead quality as assessed by the percentage of non-spherical capsules. Appendix figure 2.4 shows that the average diameter and size distribution of the Ca-alginate capsules decreased, while the proportion of capsules with non-spherical shapes increased, with increasing annular air speed. Non-spherical capsules typically had tails that may increase immune responses. For all subsequent experiments, an air speed of

about 8 m/s was chosen to form ca 500 micrometer capsules with very few non-spherical capsules. Liquid flow rate had little effect on capsule diameter or quality (results not shown), and was kept constant at 8mL/hr.

Ca-Alginate capsules were coated with PLL (15 - 30 kDa) to limit permeability and to introduce the primary amines needed for covalent crosslinking. The resulting alginate/PLL shell complex was then crosslinked by exposure to PMM<sub>50</sub> solutions, which reduces cationic charge density and generates additional succinate anions as described previously.<sup>15</sup> The corresponding chemistry is shown in supporting information Appendix Scheme 2.1.

Formation of crosslinked shells was confirmed by treating the resulting INS-1E -containing Alg-PLL-PMM<sub>50</sub> capsules with 1M Na-Citrate to chelate Ca<sup>2+</sup> ions and liquify the alginate matrix, followed by treatment with 0.1M NaOH to deprotonate the PLL layer.<sup>15</sup> Figure 2.1A shows brightfield transmittance images of as-formed Alg-PLL-PMM<sub>50</sub> capsules. Citrate treatment removes the interior calcium alginate gel and leads to partial collapse of the resulting crosslinked but hollow PLL/PMM<sub>50</sub> shells (Fig. 2.1B).

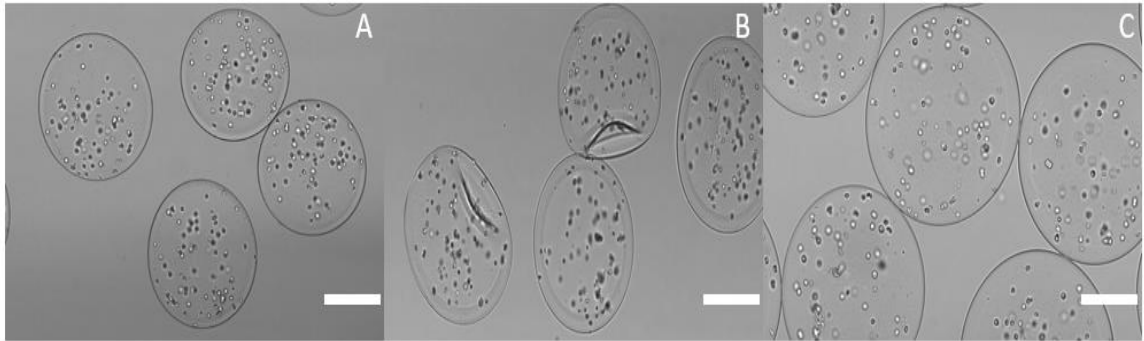


**Figure 2.1:** Transmitted light images of tests for covalent crosslinking in Alg-PLL-PMM<sub>50</sub> capsules containing INS-1E cells. A) As-formed capsules in saline; B) Capsules after treatment with 1M Na-citrate to extract calcium; C) Capsules after additional treatment with 0.1M NaOH to disrupt polyelectrolyte complex shells. Scalebar 250 $\mu$ m.

The presence of intact shells in Figure 2.1C following subsequent NaOH treatment, confirms presence of covalent crosslinking between PLL and PMM<sub>50</sub>. Their net anionic charge leads to re-expansion. The actual shell thickness as determined by confocal fluorescence microscopy using rhodamine-labelled PLL (below) is about 20 micrometer and is dictated by the depth of in-diffusion of the poly-L-lysine.

#### **2.4.2 INS-1E Cell Viability**

INS-1E cells are an adherent, glucose responsive-insulin secreting rat insulinoma cell line commonly used in diabetes research to examine beta cell function.<sup>35,36</sup> The INS-1E cells were encapsulated at  $2 \times 10^6$  cells/mL in shell-crosslinked Alg-PLL-PMM<sub>50</sub> capsules, and cell viabilities assessed over fourteen days with LIVE/DEAD fluorescent staining

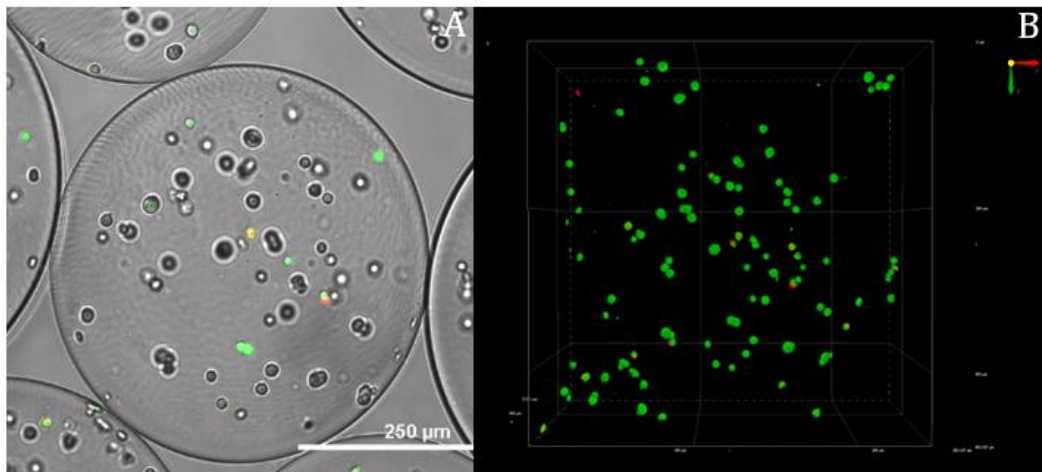


**Figure 2.2:** Cell viability: Day 0 INS-1E cells in covalently crosslinked Alg-PLL-PMM<sub>50</sub> capsules with LIVE/DEAD staining: A) equatorial FITC and TRITC confocal sections plus transmitted channel; B) corresponding top-down alpha blending 3D projection of two-channel confocal stack.

Figure 2.2A shows a representative Day 0 three-channel image formed by merging confocal equatorial sections in the FITC and TRITC channel with the transmitted light channel. Fig. 2.2B shows a 3D presentation of a full stack covering the same area of interest, without the transmitted light channel. Appendix Table 2.1 shows near-constant INS-1E cell viabilities of about 80% in capsules over three days post-encapsulation, comparable with viabilities seen in other hydrogel encapsulated INS-1E cells.<sup>37,38</sup>

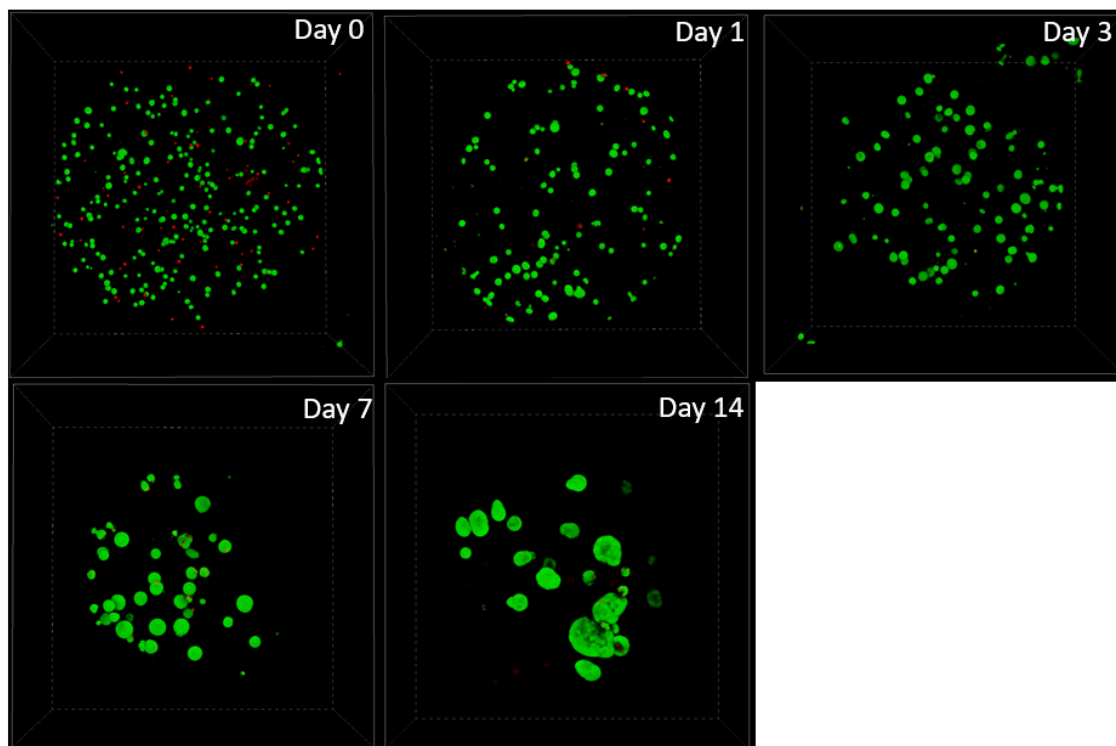


**Figure 2.3:** Progressive clustering of INS-1E cells in covalently crosslinked Alg-PLL-PMM<sub>50</sub> capsules at days 0, 1, 3, 7 and 14, shown using top-down alpha blending 3D two-channel confocal stacks, and cells stained with Calcein-AM and Ethidium Homodimer

By day 7 and especially by day 14, the INS-1E cells formed cellular spheroids (Fig. 2.3), a known feature of INS-1E cells cultured in a low attachment environment.<sup>39</sup> To verify, day 14 INS-1E capsules were stained with Hoechst 33342 (Appendix Figure 2.2). The Hoechst stained clusters revealed multiple nuclei within a cellular cluster. While these multi-cellular spheroids were fully life-stained with Calcein AM, it was not possible to reliably extract actual cell numbers. Qualitative comparison of Calcein AM and Ethidium homodimer channels on Day 7 and 14 do however clearly show that the encapsulated INS-

1E cells maintained good viabilities.

The decrease in the number and increase in size of cell clusters seen from Day 7 to Day 14 suggests that the INS-1E cells migrate towards each other to form cellular clusters. These experiments also demonstrate that the Alg-PLL-PMM<sub>50</sub> capsule technology is compatible with INS-1E cells. Future experiments will be designed to compare glucose-triggered insulin release from free and encapsulated cells.

Prior to this however, we thought it was critical to explore the radial distribution of cells within the capsules. Two questions motivated this study: the possible interference of the PLL with cells located near the capsule surface, and a desire to quantify the cells protruding from capsule surfaces. Cellular protrusion is a key problem in encapsulation as it enables contact immune recognition for the patient's immune system, increases capsule surface roughness which is correlated with increased immune response, may compromise capsule mechanical integrity, and increases chances of cell escape from the capsules. Currently, with most cell encapsulation systems, as stated by Paul de Vos, "protrusion of cells is more the rule than an exception".<sup>22</sup>

### **2.3.3 Radial Position Distribution of INS1E cells by Fluorescence Colocalization**

To simultaneously visualize the primary PLL/alginate shell and the



encapsulated INS-1E cells, Alg-PLL-PMM<sub>50</sub> capsules were prepared with fluorescently labeled PLLr and the cells were stained with Calcein AM. Calcein AM enters live cells where it becomes hydrolyzed by intracellular esterases to form a cytosol-resident fluorescent anion.

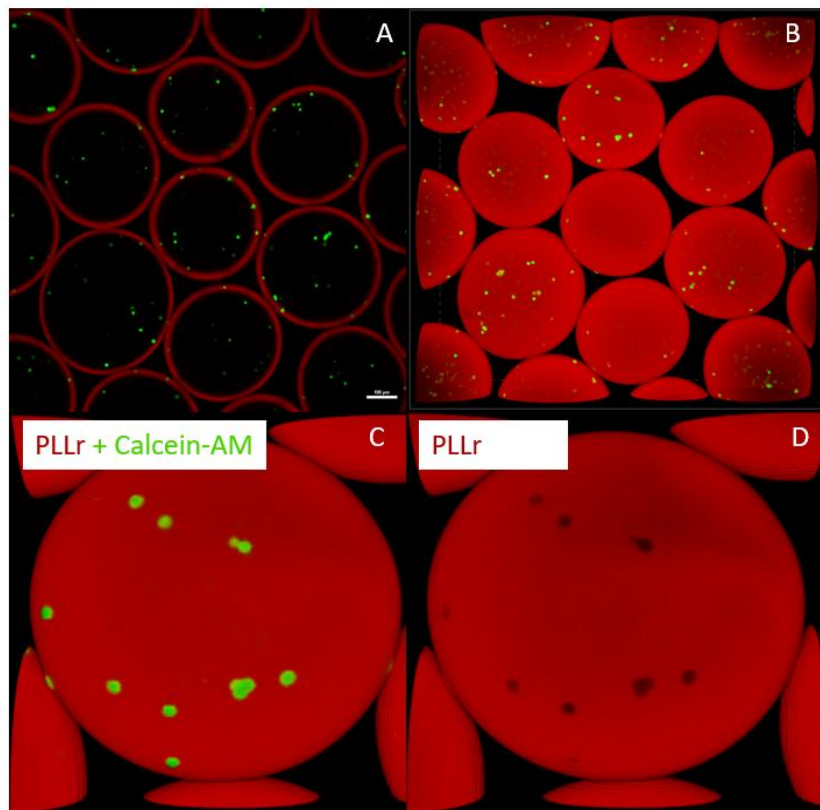


**Figure 2.4:** 2D and 3D imaging of INS-1E cells located near the surfaces of covalently crosslinked Alg-PLLr-PMM<sub>50</sub> capsules. A: Two-channel confocal equatorial section of Calcein AM stained INS-1E cells; B: corresponding 3D rendered image; C, D: comparison of two-channel (FITC and TRITC) and single-channel (TRITC) 3D rendered images, respectively, revealing cell-sized areas with lower PLLr concentration in D that correspond with cell positions shown in C.

Figure 2.4A shows the two-channel confocal fluorescence equatorial

sections of multiple capsules, while Fig. 2.4B shows the corresponding 3D rendered view. Both Fig. 2.4A and 2.4B reveal a certain fraction of (green) cells overlapping with the (red) PLLr shell, and possibly protruding from the outer capsule surface. Fig. 2.4C compares an enlarged area of the two-channel 3D view in 2.4B, with the corresponding TRITC channel, revealing areas of lower PLLr coverage (holes) of the capsules coinciding with the position of Calcein-AM-stained cells. This indicates that protruding cells may interfere with mechanical integrity of the crosslinked shell and further may lead to cell-based immune responses and even cell escape from the capsules. The quantitative live staining of the cells found in contact with the PLL-PMM<sub>50</sub> shell confirms that this shell is not toxic to the INS-1E cells. Although dead staining was not used, it is expected that non-viable cells would also show similar holes in the PLLr, which was indeed seen only in very low percentages.

Below we describe fluorescence methods designed to quantitate both the fraction of cells located within the PLLr-labelled shells, and the fraction of cells physically protruding from the capsule surface, using colocalization. The average PLLr/PMM<sub>50</sub> shell thickness was found to be 19.3 $\mu$ m (sd 4.8 $\mu$ m), and the average cell diameter was 11.5 $\mu$ m (sd 2.3 $\mu$ m).

Figure 2.5 shows the images of Calcein-AM stained live cells and the PLLr-labelled shells. Fig. 2.5A shows the as-measured equatorial two-channel

section. Fig. 2.5B shows the corresponding composite thresholded image showing cells and capsule shells. Fig. 2.5C shows the output of nearest neighbor colocalization by binary operations on a 2D section that would show zero nearest edge to edge in DiAna. This approach was then applied to complete z-stacks of two channel images, in order to sample positional information for more cells within each capsule.

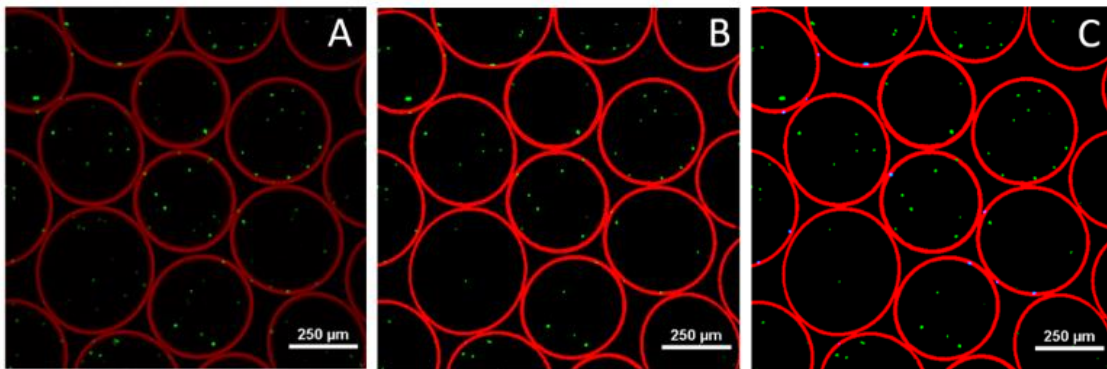


**Figure 2.5:** Protrusion mapping using cell-to-PLLr shell distances in INS-1E containing crosslinked Alg-PLLr-PMM<sub>50</sub> capsules: A) As-obtained two-channel confocal equatorial cross section; B) Binary map derived from thresholding image A in both channels; C) Binary map with cells in contact with PLLr layer marked blue.

The combined percentage of shell-resident plus protruding cells was defined as the number of cells with a zero nearest-edge-to-edge distance to the PLLr-loaded shell. This includes all cells that are found fully within this PLLr shell as well as cells that are just in contact with the inner layer of this shell. For an average PLL shell with a thickness of 19.3 $\mu\text{m}$  and an average cell diameter of 11.5 $\mu\text{m}$ , cells considered protruding into the PLLr layer or from the actual capsule surface, are ones with their center located within 25.05 $\mu\text{m}$  from the bead

surface.

For Alg-PLL-PMM<sub>50</sub> capsules with an average bead diameter of 500 $\mu$ m, this 25.05 $\mu$ m thick outer layer accounts for 27% of the total capsule volume. The fraction of cells determined to reside in this shell region was 29.8%. This close correspondence suggests a random distribution of cells throughout the volume of the calcium alginate capsule formed. This in turn suggests that a 500 $\mu$ m diameter bead would have approximately 6.7% of total cells located with their centers 5.75 $\mu$ m or less from the bead surface, i.e., actually protruding from the outermost capsule.

To assess this hypothesis, the percentage of physically protruding cells was measured by an analogous automated 3D DiAna colocalization analysis based on distance between Calcein AM stained cells in capsules, and Dex-f labelled continuous phase surrounding the capsules (Figure 2.6). The size exclusion of 2 MDa Dex-f in the supernatant from the capsules, generates contrast between the interior of the capsules and the fluorescent supernatant that can be used to create a segmented object representing the bead surface that is one pixel wide. The amount of cellular protrusion measured using this method was found to be ~7.5% which is in agreement with the manual counting.

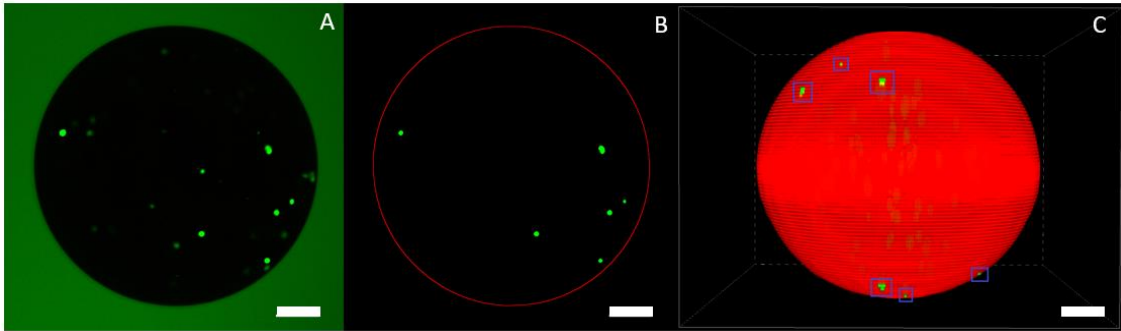


**Figure 2.6:** Protrusion mapping using cell-to-continuous media distances in INS-1E containing crosslinked Alg-PLLr-PMM<sub>50</sub> capsules: A) Single-channel confocal equatorial section showing LIVE-stained cells and continuous media containing 2 MDa Dex-f (Contrast increased) B) Binary two-channel map obtained from image A by thresholding cells and defining a single pixel-thick layer of continuous media at capsule surface (red circle); C) Alpha blending 3D projection of image B with protruding cells (cells contacting continuous media) outlined in blue squares. Scale bar 100 $\mu$ m.

To confirm the Dex-f DiAna analysis, the fraction of physically protruding Calcein-AM stained cells was also determined manually by analysis of all cells within z-stacks of multiple capsules. This manual count of physically protruding cells was found to be 7.5%, confirming the validity of the number obtained by automated 3D DiAna analysis of 7.3%, with both corresponding to the number of cells expected to be physically protruding from bead surface in case of random placement (**Error! Reference source not found.**).

**Table 2.1:** Percentage of cells in contact with PLLr layer, and physically protruding from capsules (n = 3. Dex-f p> 0.05).

Method	Cells in contact with PLLr	Physically Protruding cells	Interior cells
Colocalization with PLLr shell (DiAna)	29.8%±2.3	n/a	70.2%±2.3
Colocalization with Dex-f labelled media (DiAna)	n/a	7.3%±2.0	92.7%±2.0
Manual Count of physically protruding cells	n/a	7.5%±1.1%	92.5%±1.1%

These results confirm the need for careful assessment of the fraction of cells physically protruding from calcium alginate type capsules. Automated analyses based on confocal fluorescent colocalization data should help in future studies of conditions and coatings that may mitigate physical cell protrusion from such hydrogel capsules.

## 2.5 Conclusions

INS-1E cells encapsulated in calcium alginate beads coated with covalently crosslinked shells were shown to retain high viabilities, and to form multicellular clusters over six weeks post-encapsulation. Automated 2D and 3D confocal fluorescence mapping showed the fraction of cells initially located in contact with the crosslinked shells (30%), or located at the capsule surface (7%), reflecting random initial placement of cells within the capsules. Nevertheless, the covalently crosslinked capsules were shown to retain such cells out to at least six

weeks *in-vitro*.

## 2.6 Conflicts of interest

HDHS and NADB declare financial interests in patents filed on the encapsulation technology. HDHS is involved in a start-up company on cell encapsulation.

## 2.7 Acknowledgements

The authors would like to acknowledge NSERC for Discovery Grants to both A. Holloway and H. Stöver to fund this research, and Dr. Claes Wollheim (University of Geneva, Switzerland) for providing the INS-1E cell line used in this research.

## 2.8 References

- (1) Care, D.; Suppl, S. S. Children and Adolescents: Standards of Medical Care in Diabetesd2018. *Diabetes Care* **2018**, *41* (January), S126–S136. <https://doi.org/10.2337/dc18-S012>.
- (2) Care, D.; Suppl, S. S. Pharmacologic Approaches to Glycemic Treatment: Standards of Medical Care in Diabetesd2018. *Diabetes Care* **2018**, *41* (January), S73–S85. <https://doi.org/10.2337/dc18-S008>.
- (3) Shapiro, A. M. J.; Pokrywczynska, M.; Ricordi, C. Clinical Pancreatic Islet Transplantation. *Nat. Rev. Endocrinol.* **2017**, *13* (5), 268–277. <https://doi.org/10.1038/nrendo.2016.178>.
- (4) Qi, M.; Kinzer, K.; Danielson, K. K.; Martellotto, J.; Barbaro, B.; Wang, Y.; Bui, J. T.; Gaba, R. C.; Knuttinen, G.; Garcia-Roca, R.; et al. Five-Year

Follow-up of Patients with Type 1 Diabetes Transplanted with Allogeneic Islets: The UIC Experience. *Acta Diabetol.* **2014**, *51* (5), 833–843.  
<https://doi.org/10.1007/s00592-014-0627-6>.

- (5) Lim, F.; Sun, A. M. Microencapsulated Islets as Bioartificial Endocrine Pancreas. *Science* **1980**, *210* (4472), 908–910.
- (6) Steele, J. A. M.; Hallé, J.-P.; Poncelet, D.; Neufeld, R. J. Therapeutic Cell Encapsulation Techniques and Applications in Diabetes. *Adv. Drug Deliv. Rev.* **2014**, *67–68*, 74–83. <https://doi.org/10.1016/j.addr.2013.09.015>.
- (7) Nakayama, M. Insulin as a Key Autoantigen in the Development of Type 1 Diabetes. *Diabetes. Metab. Res. Rev.* **2011**, *27* (8), 773–777.  
<https://doi.org/10.1002/dmrr.1250>.
- (8) Vaithilingam, V.; Kollarikova, G.; Qi, M.; Larsson, R.; Lacik, I.; Formo, K.; Marchese, E.; Oberholzer, J.; Guillemin, G. J.; Tuch, B. E. Beneficial Effects of Coating Alginate Microcapsules with Macromolecular Heparin Conjugates-in Vitro and in Vivo Study. *Tissue Eng. Part A* **2014**, *20* (1–2), 324–334. <https://doi.org/10.1089/ten.TEA.2013.0254>.
- (9) Spasojevic, M.; Paredes-Juarez, G. A.; Vorenkamp, J.; de Haan, B. J.; Schouten, A. J.; de Vos, P. Reduction of the Inflammatory Responses against Alginate-Poly-L-Lysine Microcapsules by Anti-Biofouling Surfaces of PEG-b-PLL Diblock Copolymers. *PLoS One* **2014**, *9* (10), e109837.



<https://doi.org/10.1371/journal.pone.0109837>.

- (10) Rokstad, A. M.; Brekke, O.-L.; Steinkjer, B.; Ryan, L.; Kolláriková, G.; Strand, B. L.; Skjåk-Bræk, G.; Lambris, J. D.; Lacík, I.; Mollnes, T. E.; et al. The Induction of Cytokines by Polycation Containing Microspheres by a Complement Dependent Mechanism. *Biomaterials* **2013**, *34* (3), 621–630. <https://doi.org/10.1016/j.biomaterials.2012.10.012>.
- (11) Dusseault, J.; Tam, S. K.; Ménard, M.; Polizu, S.; Jourdan, G.; Yahia, L.; Hallé, J.-P. Evaluation of Alginate Purification Methods: Effect on Polyphenol, Endotoxin, and Protein Contamination. *J. Biomed. Mater. Res. Part A* **2006**, *76A* (2), 243–251. <https://doi.org/10.1002/jbm.a.30541>.
- (12) Paredes-Juarez, G. A.; de Haan, B. J.; Faas, M. M.; de Vos, P. The Role of Pathogen-Associated Molecular Patterns in Inflammatory Responses against Alginate Based Microcapsules. *J. Control. Release* **2013**, *172* (3), 983–992. <https://doi.org/10.1016/j.jconrel.2013.09.009>.
- (13) Mørch, Ý. A.; Donati, I.; Strand, B. L.; Skjåk-Bræk, G. Molecular Engineering as an Approach to Design New Functional Properties of Alginate. *Biomacromolecules* **2007**, *8* (9), 2809–2814. <https://doi.org/10.1021/bm700502b>.
- (14) Vegas, A. J.; Veisoh, O.; Doloff, J. C.; Ma, M.; Tam, H. H.; Bratlie, K.; Li, J.; Bader, A. R.; Langan, E.; Olejnik, K.; et al. Combinatorial Hydrogel Library

Enables Identification of Materials That Mitigate the Foreign Body Response in Primates. *Nat. Biotechnol.* **2016**, *34* (3), 345–352. <https://doi.org/10.1038/nbt.3462>.

- (15) Gardner, C. M.; Potter, M. A.; Stöver, H. D. H. Improving Covalent Cell Encapsulation with Temporarily Reactive Polyelectrolytes. *J. Mater. Sci. Mater. Med.* **2012**, *23* (1), 181–193. <https://doi.org/10.1007/s10856-011-4523-0>.
- (16) Dusseault, J.; Langlois, G.; Meunier, M.-C.; Ménard, M.; Perreault, C.; Hallé, J.-P. The Effect of Covalent Cross-Links between the Membrane Components of Microcapsules on the Dissemination of Encapsulated Malignant Cells. *Biomaterials* **2008**, *29* (7), 917–924. <https://doi.org/10.1016/j.biomaterials.2007.10.045>.
- (17) Bhujbal, S. V; de Haan, B.; Niclou, S. P.; de Vos, P. A Novel Multilayer Immunoisolating Encapsulation System Overcoming Protrusion of Cells. *Sci. Rep.* **2014**, *4*, 6856. <https://doi.org/10.1038/srep06856>.
- (18) Kamperman, T.; Henke, S.; Visser, C. W.; Karperien, M.; Leijten, J. Centering Single Cells in Microgels via Delayed Crosslinking Supports Long-Term 3D Culture by Preventing Cell Escape. *Small* **2017**, *13* (22), 1603711. <https://doi.org/10.1002/smll.201603711>.
- (19) Lienemann, P. S.; Rossow, T.; Mao, A. S.; Vallmajo-Martin, Q.; Ehrbar, M.;

Mooney, D. J. Single Cell-Laden Protease-Sensitive Microniches for Long-Term Culture in 3D. *Lab Chip* **2017**, *17* (4), 727–737.

<https://doi.org/10.1039/C6LC01444E>.

- (20) Hoesli, C. A.; Kiang, R. L. J.; Mocinecová, D.; Speck, M.; Mošková, D. J.; Donald-Hague, C.; Lacík, I.; Kieffer, T. J.; Piret, J. M. Reversal of Diabetes by BTC3 Cells Encapsulated in Alginate Beads Generated by Emulsion and Internal Gelation. *J. Biomed. Mater. Res. Part B Appl. Biomater.* **2012**, *100B* (4), 1017–1028. <https://doi.org/10.1002/jbm.b.32667>.
- (21) Hoesli, C. A.; Kiang, R. L. J.; Raghuram, K.; Pedroza, R. G.; Markwick, K. E.; Colantuoni, A. M. R.; Piret, J. M. Mammalian Cell Encapsulation in Alginate Beads Using a Simple Stirred Vessel. *J. Vis. Exp.* **2017**, No. 124. <https://doi.org/10.3791/55280>.
- (22) Bhujbal, S. V.; de Haan, B.; Niclou, S. P.; de Vos, P. A Novel Multilayer Immunoisolating Encapsulation System Overcoming Protrusion of Cells. *Sci. Rep.* **2015**, *4* (1), 6856. <https://doi.org/10.1038/srep06856>.
- (23) Ma, M.; Chiu, A.; Sahay, G.; Doloff, J. C.; Dholakia, N.; Thakrar, R.; Cohen, J.; Vegas, A.; Chen, D.; Bratlie, K. M.; et al. Core-Shell Hydrogel Microcapsules for Improved Islets Encapsulation. *Adv. Healthc. Mater.* **2013**, *2* (5), 667–672. <https://doi.org/10.1002/adhm.201200341>.
- (24) Safley, S. A.; Kenyon, N. S.; Berman, D. M.; Barber, G. F.; Willman, M.;

- Duncanson, S.; Iwakoshi, N.; Holdcraft, R.; Gazda, L.; Thompson, P.; et al. Microencapsulated Adult Porcine Islets Transplanted Intraperitoneally in Streptozotocin-Diabetic Non-Human Primates. *Xenotransplantation* **2018**, e12450. <https://doi.org/10.1111/xen.12450>.
- (25) Kleinberger, R. M.; Burke, N. A. D.; Zhou, C.; Stöver, H. D. H. Synthetic Polycations with Controlled Charge Density and Molecular Weight as Building Blocks for Biomaterials. *J. Biomater. Sci. Polym. Ed.* **2016**, *27* (4), 351–369. <https://doi.org/10.1080/09205063.2015.1130407>.
- (26) Schindelin, J.; Arganda-Carreras, I.; Frise, E.; Kaynig, V.; Longair, M.; Pietzsch, T.; Preibisch, S.; Rueden, C.; Saalfeld, S.; Schmid, B.; et al. Fiji: An Open-Source Platform for Biological-Image Analysis. *Nat. Methods* **2012**, *9* (7), 676–682. <https://doi.org/10.1038/nmeth.2019>.
- (27) Ollion, J.; Cochenec, J.; Loll, F.; Escudé, C.; Boudier, T. TANGO: A Generic Tool for High-Throughput 3D Image Analysis for Studying Nuclear Organization. *Bioinformatics* **2013**, *29* (14), 1840–1841. <https://doi.org/10.1093/bioinformatics/btt276>.
- (28) Gilles, J.-F.; Dos Santos, M.; Boudier, T.; Bolte, S.; Heck, N. DiAna, an ImageJ Tool for Object-Based 3D Co-Localization and Distance Analysis. *Methods* **2017**, *115*, 55–64. <https://doi.org/10.1016/J.YMETH.2016.11.016>.
- (29) JANÁČEK, J.; KREFT, M.; ČEBAŠEK, V.; ERŽEN, I. Correcting the Axial

Shrinkage of Skeletal Muscle Thick Sections Visualized by Confocal Microscopy. *J. Microsc.* **2012**, *246* (2), 107–112.  
<https://doi.org/10.1111/j.1365-2818.2011.03594.x>.

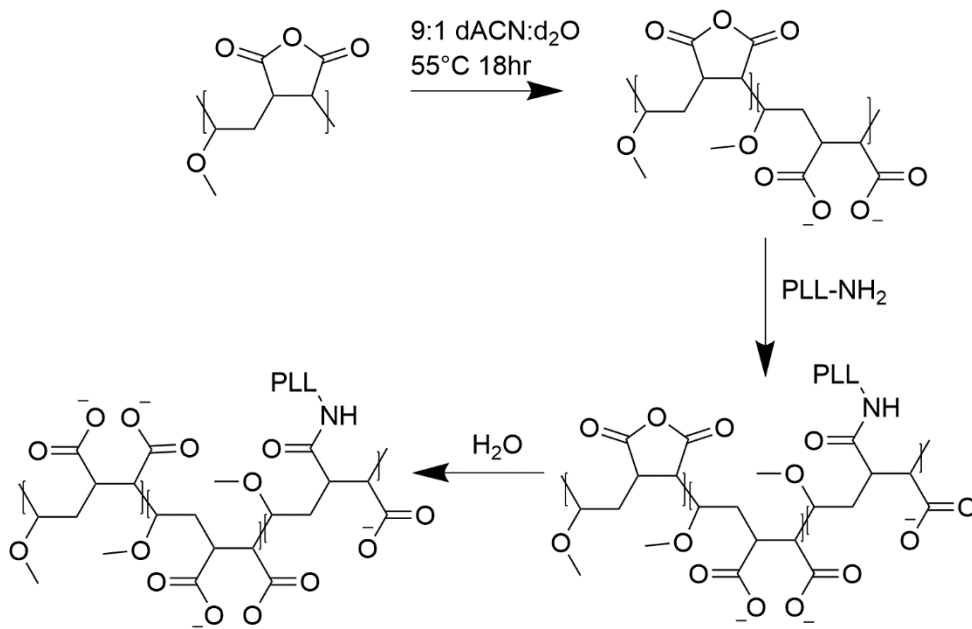
- (30) Andersen, T.; Auk-Emblem, P.; Dornish, M. 3D Cell Culture in Alginate Hydrogels. *Microarrays (Basel, Switzerland)* **2015**, *4* (2), 133–161.  
<https://doi.org/10.3390/microarrays4020133>.
- (31) Canaple, L.; Rehor, A.; Hunkeler, D. Improving Cell Encapsulation through Size Control. *J. Biomater. Sci. Polym. Ed.* **2002**, *13* (7), 783–796.
- (32) Veisoh, O.; Doloff, J. C.; Ma, M.; Vegas, A. J.; Tam, H. H.; Bader, A. R.; Li, J.; Langan, E.; Wyckoff, J.; Loo, W. S.; et al. Size- and Shape-Dependent Foreign Body Immune Response to Materials Implanted in Rodents and Non-Human Primates. *Nat. Mater.* **2015**, *14* (6), 643–651.  
<https://doi.org/10.1038/nmat4290>.
- (33) De Vos, P.; De Haan, B.; Pater, J.; Van Schilfgaard, R. Association between Capsule Diameter, Adequacy of Encapsulation, and Survival of Microencapsulated Rat Islet Allografts. *Transplantation* **1996**, *62* (7), 893–899.
- (34) Strand, B. L.; Gåserød, O.; Kulseng, B.; Espevik, T.; Skjåk-Bræk, G. Alginate-Polylysine-Alginate Microcapsules: Effect of Size Reduction on Capsule Properties. *J. Microencapsul.* **2002**, *19* (5), 615–630.

<https://doi.org/10.1080/02652040210144243>.

- (35) Merglen, A.; Theander, S.; Rubi, B.; Chaffard, G.; Wollheim, C. B.; Maechler, P. Glucose Sensitivity and Metabolism-Secretion Coupling Studied during Two-Year Continuous Culture in INS-1E Insulinoma Cells. *Endocrinology* **2004**, *145* (2), 667–678. <https://doi.org/10.1210/en.2003-1099>.
- (36) Skelin, M.; Rupnik, M.; Cencic, A. Pancreatic Beta Cell Lines and Their Applications in Diabetes Mellitus Research. *ALTEX* **2010**, *27* (2), 105–113.
- (37) Espona-Noguera, A.; Ciriza, J.; Cañibano-Hernández, A.; Fernandez, L.; Ochoa, I.; Saenz del Burgo, L.; Pedraz, J. L. Tunable Injectable Alginate-Based Hydrogel for Cell Therapy in Type 1 Diabetes Mellitus. *Int. J. Biol. Macromol.* **2018**, *107*, 1261–1269.  
<https://doi.org/10.1016/J.IJBIOMAC.2017.09.103>.
- (38) Marchioli, G.; van Gurp, L.; van Krieken, P. P.; Stamatialis, D.; Engelse, M.; van Blitterswijk, C. A.; Karperien, M. B. J.; de Koning, E.; Alblas, J.; Moroni, L.; et al. Fabrication of Three-Dimensional Bioplotting Hydrogel Scaffolds for Islets of Langerhans Transplantation. *Biofabrication* **2015**, *7* (2), 025009. <https://doi.org/10.1088/1758-5090/7/2/025009>.
- (39) Hilderink, J.; Spijker, S.; Carlotti, F.; Lange, L.; Engelse, M.; van Blitterswijk, C.; de Koning, E.; Karperien, M.; van Apeldoorn, A. Controlled

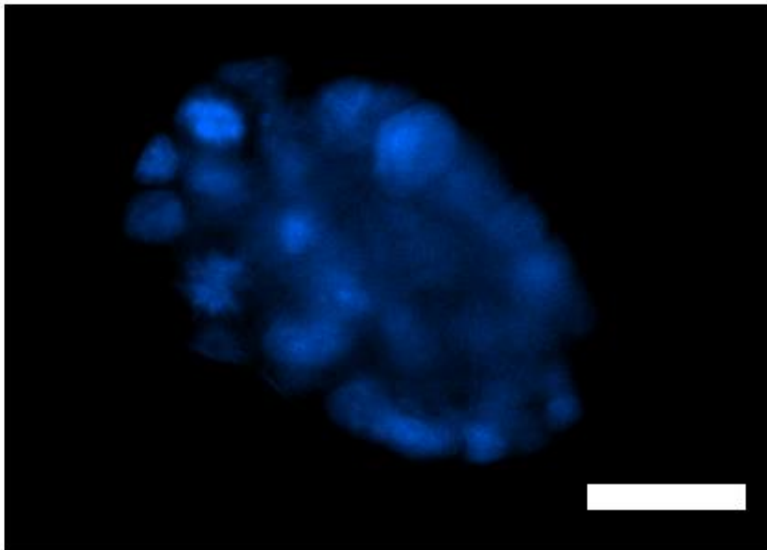
Aggregation of Primary Human Pancreatic Islet Cells Leads to Glucose-Responsive Pseudoislets Comparable to Native Islets. *J. Cell. Mol. Med.* **2015**, *19* (8), 1836–1846. <https://doi.org/10.1111/jcmm.12555>.

## 2.9 Appendix



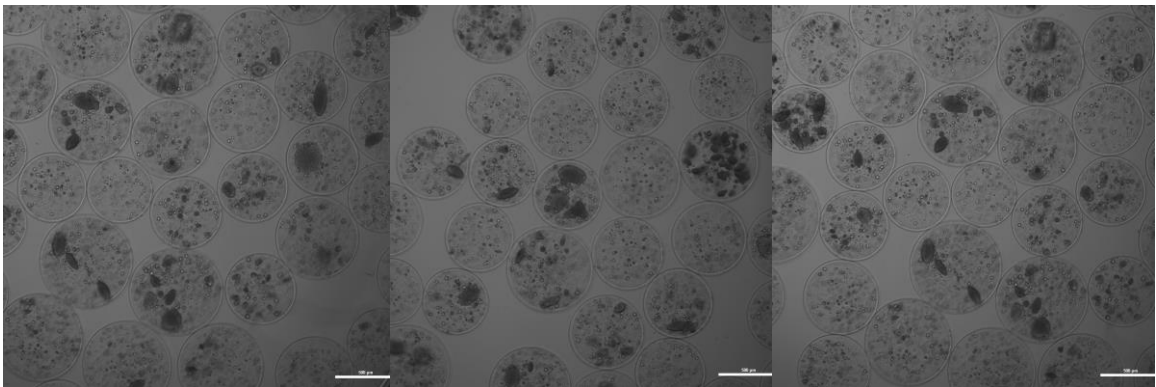
Appendix Scheme 2.1: Crosslinking Chemistry for A-PLL-PMM<sub>50</sub> Capsules.

The maleic anhydride groups of the PMM<sub>50</sub> undergo a nucleophilic ring opening by the primary amines of the PLL coating, reducing the cationic charge density by formation of amide bonds and creating a covalently crosslinking shell. The unreacted maleic anhydride groups subsequently spontaneously hydrolyze to form succinate anions.



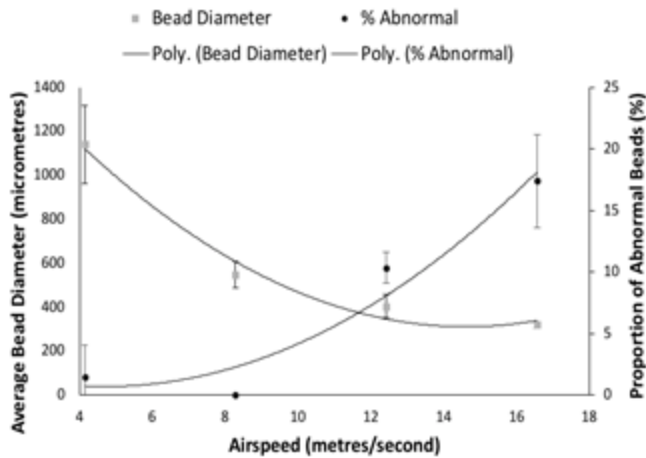
Appendix Figure 2.1: Day 14 INS-1E cell cluster stained with Hoechst 3342. Scale bar 25 $\mu$ m.

To confirm the formation of cellular clusters, Day 14 Alg-PLL-PMM<sub>50</sub> capsules were stained with 50 $\mu$ L of 10 $\mu$ m Hoechst 3342 for 20 minutes and imaged on a Nikon Ti eclipse inverted microscope. Cell clusters show staining of multiply nuclei confirming the formation of cell clusters.

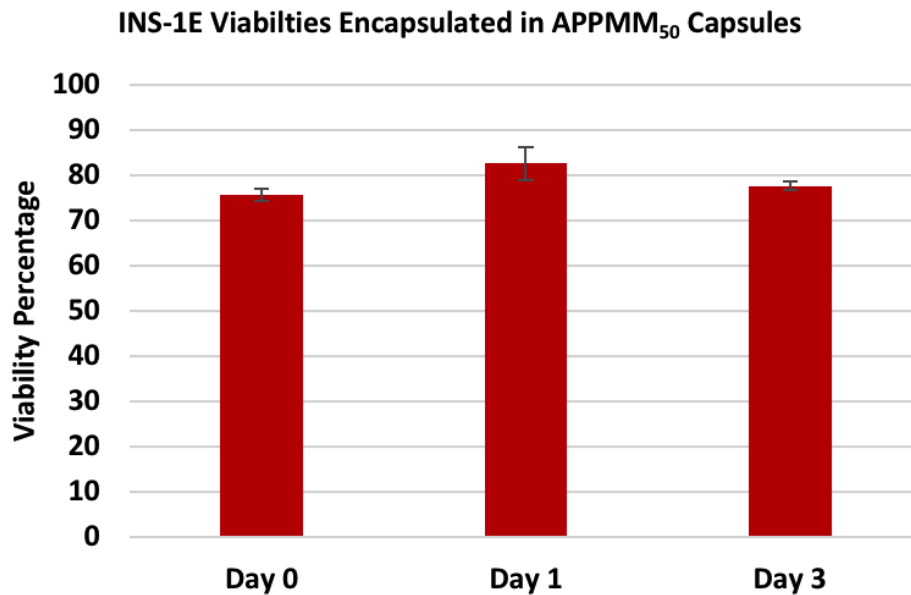


Appendix Figure 2.2: Inverted brightfield image of Day 42 INS-1E cells (scalebar 500 $\mu$ m)





Appendix Figure 2.3: Average capsule diameter and percent non-spherical capsules as function of coaxial air flow. Lines are second order polynomial trendlines fitted to the data points to help guide the eye. Experiments were carried out in triplicates, with 30 capsules measured for each sample.



Appendix Table 2.1: Cell viabilities of INS-1E encapsulated cells at days 0, 1, and 3. p-values > 0.05

## Chapter 3 – Diels Alder Reactive Charge-Shifting Polycations

Mitchell A. Johnson<sup>a</sup>, Samantha Ros<sup>a</sup>, Harald D.H. Stöver<sup>a\*</sup>

<sup>a</sup>*Dept. of Chemistry and Chemical Biology, McMaster University, Hamilton, ON, Canada:*

### 3.0 Introduction

The transplantation of cell secreting therapeutic agents is a promising approach to treatment of many enzyme and hormonal deficiency disorders as well as other disease such as Type 1 Diabetes<sup>1</sup> and Hemophilia<sup>2</sup>, as well as Parkinson's<sup>3</sup>. In this approach cells capable of secreting a therapeutic enzyme or hormone are encapsulated within a semipermeable membrane that provides a synthetic extra cellular matrix that allows for nutrient diffusion while providing physical isolation of the cells from a patient's immune system<sup>4</sup>.

The most commonly used cell encapsulation system is based on alginate/poly-L-lysine/alginate (APA) beads<sup>1,5-8</sup>. APA beads are composed of an polyanionic alginate core crosslinked by divalent cations such as calcium that is then coated with a polycation such as poly-L-lysine to control capsule permeability and improve stability and then is coated with an additional layer of Na-Alginate to reduce surface cationic charge density of un-complexed cationic patches<sup>1</sup>. While these capsules are shown to initially perform well *in vivo*, *in vivo* exchange of calcium for sodium leads to capsule weakening over time that can result in capsule rupture. Loss of the polyanionic overcoat can also expose

patches of polycations at the surface that eventually lead to an immune response that compromises the capsules' long-term function<sup>9-11</sup>.

Long-term stability can be introduced by incorporating covalent crosslinking into the capsules. Covalently crosslinked shells formed by the reaction of polycations with polyanions bearing reactive groups, or synthetic polycations with reduced cationic charge density crosslinked by small molecule crosslinkers, have been shown to have improved mechanical robustness, antifouling properties, and immuno-isolation function over conventional APA capsules.<sup>12-18</sup> A complementary approach to crosslinked shells involves introducing covalent crosslinking into the bead to reinforce the cell-containing Ca-alginate core. Interpenetrating gel networks based on synthetic hydrogels crosslinked within calcium alginate beads have been explored as a method of tuning the physiochemical properties of calcium alginate beads while also providing encapsulated cells with a long term permanent hydrogel matrix<sup>19-22</sup>.

Here we explore new versions of Diels-Alder-crosslinkable gel-formers based on diene-functional acrylic copolymers. The Diels-Alder reaction is a click reaction that has been increasingly used in biomaterials due to its ability to react under aqueous conditions without the need of potentially cytotoxic small molecules.<sup>23-26</sup> These new copolymers consist of N,N-(dimethylamino) ethyl acrylate (DMAEA) and Furfuryl acrylamide (FFAm). DMAEA is charge-shifting cationic monomer capable of spontaneous hydrolysis into carboxylates under

physiological conditions.<sup>18,27,28</sup> This charge-shifting behavior allows for complexation with polyanions and in the case of cell encapsulation, it can be complexed to the alginate capsule surface and crosslinked in place, with subsequent hydrolysis reducing cationic charge density.<sup>18</sup> These copolymers will be used to form capsules with covalently crosslinked shells and cores. The reactive polycation coated onto the surface can be crosslinked by addition of a bifunctional maleimide crosslinker or a maleimide functional poly(methyl vinyl ether-alt-maleic acid) polyanion.<sup>23,25</sup> Additionally, lower molecular weight copolymers may be introduced into preformed Ca-alginate beads by inward diffusion and crosslinked by crosslinkers as described above.<sup>21</sup> In both cases, the complexation of the reactive polycation is expected to preconcentrate the reactive groups, accelerating the subsequent crosslinking reaction to produce capsules with improved long-term stability and cytocompatibility.

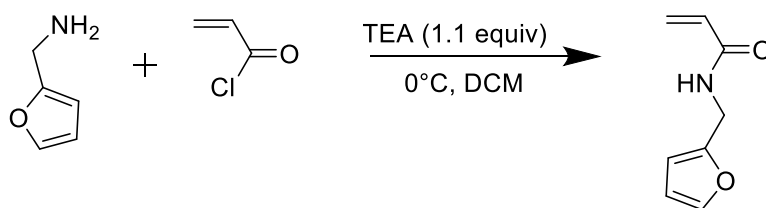
## **3.1 Experimental**

### **3.11 Materials**

All materials were used as received unless stated otherwise. N,N-(dimethylamino)ethyl acrylate (98%), Furfuryl amine (>99%), Acryoyl Chloride (>97%) were purchased from Sigma-Aldrich. DMSO-*d*6 (99.9 %) was purchased from Cambridge Isotope Laboratories Inc. Dichloromethane was purchased

from Caledon Laboratory Chemicals Azobis(isobutyronitrile) (AIBN) (>99 %) was purchased from Dupont.

### 3.12 Synthesis of Furfurylacrylamide (FFAm)



**Scheme 3.1:** Synthesis of FFAm by amidation reaction of acryloyl chloride with furfurylamine.

To a 100ml round-bottom flask containing 50ml of dry dichloromethane, furfurylamine (1.00g, 10.29mmol) and triethylamine (TEA) (1.14g, 11.3mmol) were added and the mixture was cooled for 30mins at 0°C in an ice water bath. Subsequently, acryloyl chloride (1.025g, 11.3mmol) was added dropwise over 5 mins under stirring. The reaction mixture was allowed to warm to room temperature and was then stirred overnight. The crude reaction mixture was transferred to a separatory funnel and the organic layer washed with 5%w/v sodium bicarbonate (3x, 100ml), then brine (1x,100ml), and dried over anhydrous Na<sub>2</sub>SO<sub>4</sub>. The dried solution was concentrated *in vacuo* by rotatory evaporation to

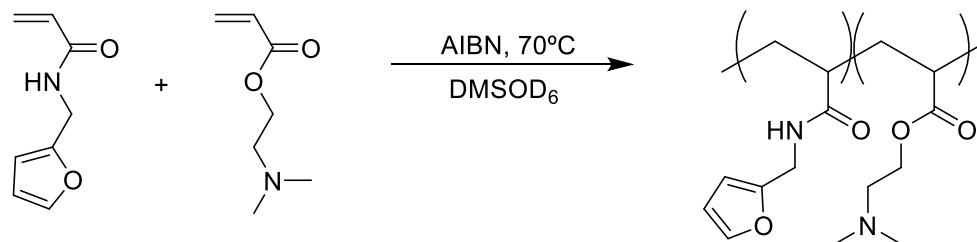
produce a yellow viscous liquid, which was then dried under a stream of N<sub>2</sub> gas overnight to yield FFAm as a pale yellow solid (0.87g, 59.5%).

### 3.13 Reactivity Ratios

A series of NMR scale copolymer solutions of N,N-(dimethylamino) ethyl acrylate (DMAEA) and FFAm were prepared at 10%w/v monomer loading in 0.83mL of DMSO D6 with 1 mol% of AIBN relative to total monomer loading with initial feed ratios 90:10, 75:25, 50:50, 25:75 and 10:90. The copolymer solutions were heated at 70°C for 5 to 60 min intervals to achieve monomer conversion steps less than 5% as monitored by <sup>1</sup>H NMR. After each heating step the copolymerizations were quenched by placing them on ice. Following quenching the <sup>1</sup>H NMR of the copolymer solutions were measured on a 500 and 600 MHz Bruker Avance spectrometer. Conversion steps were measured by the decrease in vinyl signals of DMAEA and FFAm relative to the combined N,N-dimethyl peaks of the monomer and polymer. Reactivity ratios were then determined by fitting the measured instantaneous monomer and copolymer composition to the Mayo-Lewis terminal model equation using the least-squares method with the Solver tool in Microsoft Excel.

## 3.2 Results

### 3.21 Reactivity Ratios



Scheme 3.2: NMR scale copolymerization of DMAEA and FFAm

The reactivity ratios were measured to be  $r_1 = 1.83$  for DMAEA and  $r_2 = 0.23$  for FFAm. These ratios show that there is a significant preference for incorporation of DMAEA over FFAm with DMAEA having a tendency to homopropagate and FFAm to cross-propagate. Which may be a result of the more sterically bulky furan group of the FFAm monomer. The preferential incorporation of DMAEA is also shown in copolymerization kinetics. As the amount of FFAm in the initial monomer feed is increased, there is a decrease in the total amount of monomer conversion over the same polymerization times as a result of FFAm's

preference to cross-propagate.

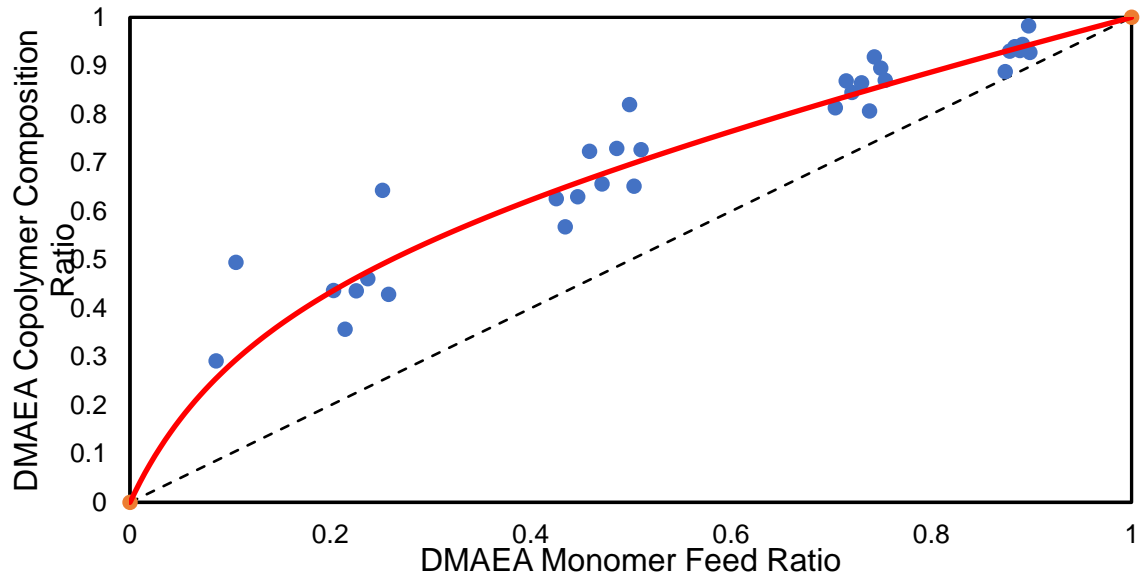


Figure 3.1: Instantaneous copolymer composition graph of DMAEA and FFAm  $r_1 = 1.828$  and  $r_2 = 0.227$



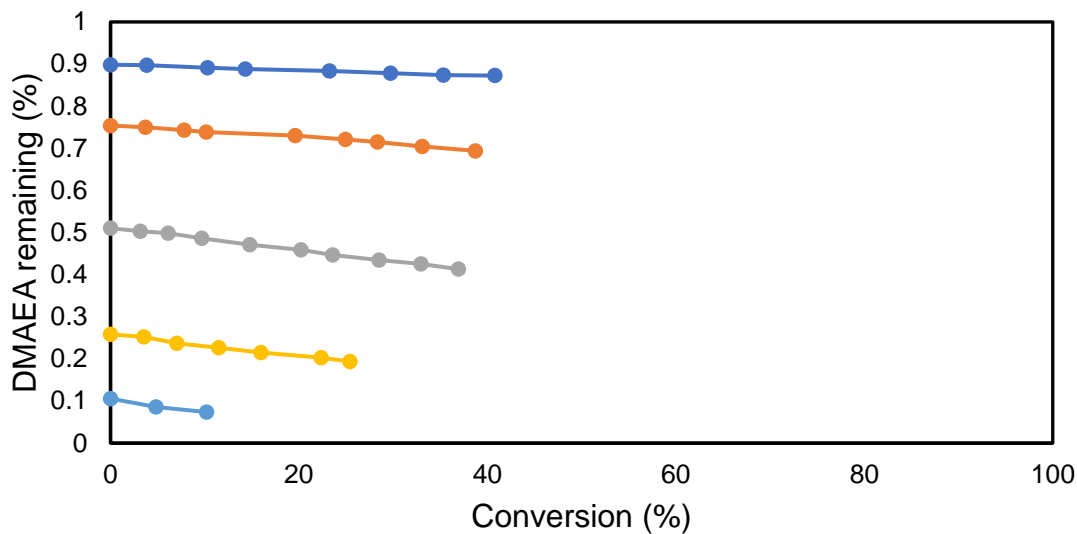


Figure 3.2: DMAEA fraction remaining in the monomer pool as a function of conversion over a series of different initial feeds of DMAEA and FFAM.

### 3.3 Future Work

Future experiments for this project would be to look at the controlled radical copolymerization of these monomers to target molecular weights as polycation size greatly effects its complexation diffusivity with Ca-alginate beads. The hydrolysis kinetics of the DMAEA side chain of copolymers with varying compositions would be measured as of PDMAEA hydrolysis plateaus and the extent of hydrolysis is affected by copolymer composition. The ability of these reactive copolymers to form covalently crosslinked shells and cores with Ca-alginate using dienophile functional crosslinkers. Additionally, the effect on permeability and stability of these capsule with the incorporated Diels-Alder covalent crosslinking will be measured. Finally, model cell encapsulation experiments should be performed to assess the degree of effect these

copolymers have on encapsulated cells

### 3.4 References

- (1) Lim, F.; Sun, A. M. Microencapsulated Islets as Bioartificial Endocrine Pancreas. *Science* **1980**, *210* (4472), 908–910.
- (2) Van Raamsdonk, J. M.; Ross, C. J. D.; Potter, M. A.; Kurachi, S.; Kurachi, K.; Stafford, D. W.; Chang, P. L. Treatment of Hemophilia B in Mice with Nonautologous Somatic Gene Therapeutics. *J. Lab. Clin. Med.* **2002**, *139* (1), 35–42. <https://doi.org/10.1067/mlc.2002.120649>.
- (3) Shoichet, M. S.; Winn, S. R. Cell Delivery to the Central Nervous System. *Adv. Drug Deliv. Rev.* **2000**, *42* (1–2), 81–102. [https://doi.org/10.1016/S0169-409X\(00\)00055-7](https://doi.org/10.1016/S0169-409X(00)00055-7).
- (4) Orive, G.; Hernández, R. M.; Gascón, A. R.; Calafiore, R.; Chang, T. M. S.; Vos, P. De; Hortelano, G.; Hunkeler, D.; Lacík, I.; Shapiro, A. M. J.; et al. Cell Encapsulation: Promise and Progress. *Nat. Med.* **2003**, *9* (1), 104–107. <https://doi.org/10.1038/nm0103-104>.
- (5) Sun, Y.; Ma, X.; Zhou, D.; Vacek, I.; Sun, A. M. Normalization of Diabetes in Spontaneously Diabetic Cynomolgus Monkeys by Xenografts of Microencapsulated Porcine Islets without Immunosuppression. *J. Clin. Invest.* **1996**, *98* (6), 1417–1422. <https://doi.org/10.1172/JCI118929>.
- (6) Strand, B. L.; Gåserød, O.; Kulseng, B.; Espevik, T.; Skjåk-Bræk, G. Alginate-Polylysine-Alginate Microcapsules: Effect of Size Reduction on

- Capsule Properties. *J. Microencapsul.* **2002**, *19* (5), 615–630.  
<https://doi.org/10.1080/02652040210144243>.
- (7) Calafiore, R. Microencapsulated Pancreatic Islet Allografts Into Nonimmunosuppressed Patients With Type 1 Diabetes: First Two Cases. *Diabetes Care* **2006**, *29* (1), 137–138.  
<https://doi.org/10.2337/diacare.29.1.137>.
- (8) Qi, M.; Kinzer, K.; Danielson, K. K.; Martellotto, J.; Barbaro, B.; Wang, Y.; Bui, J. T.; Gaba, R. C.; Knuttinen, G.; Garcia-Roca, R.; et al. Five-Year Follow-up of Patients with Type 1 Diabetes Transplanted with Allogeneic Islets: The UIC Experience. *Acta Diabetol.* **2014**, *51* (5), 833–843.  
<https://doi.org/10.1007/s00592-014-0627-6>.
- (9) Rokstad, A. M.; Donati, I.; Borgogna, M.; Oberholzer, J.; Strand, B. L.; Espevik, T.; Skjåk-Bræk, G. Cell-Compatible Covalently Reinforced Beads Obtained from a Chemoenzymatically Engineered Alginate. *Biomaterials* **2006**, *27* (27), 4726–4737.  
<https://doi.org/10.1016/j.biomaterials.2006.05.011>.
- (10) Tam, S. K.; Bilodeau, S.; Dusseault, J.; Langlois, G.; Hallé, J. P.; Yahia, L. H. Biocompatibility and Physicochemical Characteristics of Alginate-Polycation Microcapsules. *Acta Biomater.* **2011**, *7* (4), 1683–1692.  
<https://doi.org/10.1016/j.actbio.2010.12.006>.
- (11) Rokstad, A. M.; Holtan, S.; Strand, B.; Steinkjer, B.; Ryan, L.; Kulseng, B.; Skjåk-Bræk, G.; Espevik, T. Microencapsulation of Cells Producing

Therapeutic Proteins: Optimizing Cell Growth and Secretion. *Cell Transplant.* **2002**, *11* (4), 313–324.

<https://doi.org/10.3727/000000002783985774>.

- (12) Gardner, C. M.; Potter, M. A.; Stöver, H. D. H. Improving Covalent Cell Encapsulation with Temporarily Reactive Polyelectrolytes. *J. Mater. Sci. Mater. Med.* **2012**, *23* (1), 181–193. <https://doi.org/10.1007/s10856-011-4523-0>.
- (13) Gardner, C. M.; Burke, N. A. D.; Stöver, H. D. H. Cross-Linked Microcapsules Formed From Self-Deactivating Reactive Polyelectrolytes. *Langmuir* **2010**, *26* (7), 4916–4924. <https://doi.org/10.1021/la903540c>.
- (14) Jafar Mazumder, M. A.; Shen, F.; Burke, N. A. D.; Potter, M. A.; Stöver, H. D. H. Self-Cross-Linking Polyelectrolyte Complexes for Therapeutic Cell Encapsulation. *Biomacromolecules* **2008**, *9* (9), 2292–2300. <https://doi.org/10.1021/bm800580c>.
- (15) Gardner, C. M.; Burke, N. A. D.; Chu, T.; Shen, F.; Potter, M. A.; Stöver, H. D. H. Poly(Methyl Vinyl Ether-Alt-Maleic Acid) Polymers for Cell Encapsulation. *J. Biomater. Sci. Polym. Ed.* **2011**, *22* (16), 2127–2145. <https://doi.org/10.1163/092050610X535149>.
- (16) Gardner, C. M.; Stöver, H. D. H. Reactive Polyanions Based on Poly(4,4-Dimethyl-2-Vinyl-2-Oxazoline-5-One- Co -Methacrylic Acid). *Macromolecules* **2011**, *44* (18), 7115–7123. <https://doi.org/10.1021/ma201409t>.

- (17) Hastings, D. E.; Stöver, H. D. H. Crosslinked Hydrogel Capsules for Cell Encapsulation Formed Using Amino/Betaine Dual-Functional Semibatch Copolymers. *ACS Appl. Polym. Mater.* **2019**, *1* (8), 2055–2067.  
<https://doi.org/10.1021/acsapm.9b00124>.
- (18) Ros, S.; Burke, N. A. D.; Stöver, H. D. H. Synthesis and Properties of Charge-Shifting Polycations: Poly[3-Aminopropylmethacrylamide- Co -2-(Dimethylamino)Ethyl Acrylate]. *Macromolecules* **2015**, *48* (24), 8958–8970. <https://doi.org/10.1021/acs.macromol.5b02191>.
- (19) Mahou, R.; Meier, R. P. H.; Bühler, L. H.; Wandrey, C. Alginate-Poly(Ethylene Glycol) Hybrid Microspheres for Primary Cell Microencapsulation. *Mater. (Basel, Switzerland)* **2014**, *7* (1), 275–286.  
<https://doi.org/10.3390/ma7010275>.
- (20) Mahou, R.; Kolláriková, G.; Gonelle-Gispert, C.; Meier, R.; Schmitt, F.; Tran, N. M.; Dufresne, M.; Altimari, I.; Lacík, I.; Bühler, L.; et al. Combined Electrostatic and Covalent Polymer Networks for Cell Microencapsulation. *Macromol. Symp.* **2013**, *329* (1), 49–57.  
<https://doi.org/10.1002/masy.201200099>.
- (21) Mazumder, M. A. J.; Burke, N. A. D.; Shen, F.; Potter, M. A.; Stöver, H. D. H. Core-Cross-Linked Alginate Microcapsules for Cell Encapsulation. *Biomacromolecules* **2009**, *10* (6), 1365–1373.  
<https://doi.org/10.1021/bm801330j>.
- (22) Meier, R. P. H.; Mahou, R.; Morel, P.; Meyer, J.; Montanari, E.; Muller, Y.

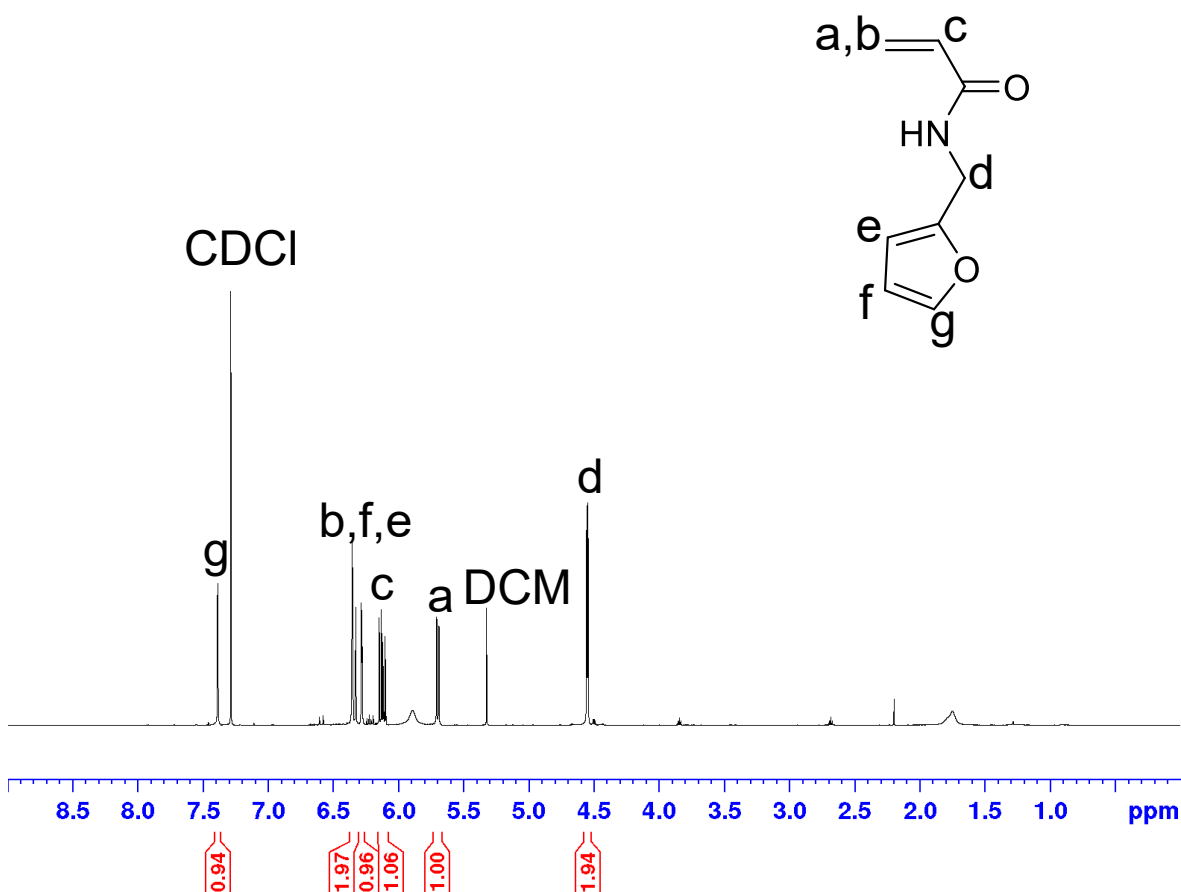
- D.; Christofilopoulos, P.; Wandrey, C.; Gonelle-Gispert, C.; Bühler, L. H. Microencapsulated Human Mesenchymal Stem Cells Decrease Liver Fibrosis in Mice. *J. Hepatol.* **2015**, *62* (3), 634–641. <https://doi.org/10.1016/j.jhep.2014.10.030>.
- (23) Stewart, S. A.; Backholm, M.; Burke, N. A. D.; Stöver, H. D. H. Cross-Linked Hydrogels Formed through Diels-Alder Coupling of Furan- and Maleimide-Modified Poly(Methyl Vinyl Ether- Alt -Maleic Acid). *Langmuir* **2016**, *32* (7), 1863–1870. <https://doi.org/10.1021/acs.langmuir.5b04450>.
- (24) Smith, L. J.; Taimoory, S. M.; Tam, R. Y.; Baker, A. E. G.; Binth Mohammad, N.; Trant, J. F.; Shoichet, M. S. Diels-Alder Click-Cross-Linked Hydrogels with Increased Reactivity Enable 3D Cell Encapsulation. *Biomacromolecules* **2018**, *19* (3), 926–935. <https://doi.org/10.1021/acs.biomac.7b01715>.
- (25) Madl, C. M.; Heilshorn, S. C. Rapid Diels-Alder Cross-Linking of Cell Encapsulating Hydrogels. *Chem. Mater.* **2019**, *31* (19), 8035–8043. <https://doi.org/10.1021/acs.chemmater.9b02485>.
- (26) Kolb, H. C.; Finn, M. G.; Sharpless, K. B. Click Chemistry: Diverse Chemical Function from a Few Good Reactions. *Angew. Chemie Int. Ed.* **2001**, *40* (11), 2004–2021. [https://doi.org/10.1002/1521-3773\(20010601\)40:11<2004::AID-ANIE2004>3.0.CO;2-5](https://doi.org/10.1002/1521-3773(20010601)40:11<2004::AID-ANIE2004>3.0.CO;2-5).
- (27) McCool, M. B.; Senogles, E. The Self-Catalysed Hydrolysis of Poly(N,N-Dimethylaminoethyl Acrylate). *Eur. Polym. J.* **1989**, *25* (7–8), 857–860.

[https://doi.org/10.1016/0014-3057\(89\)90054-2](https://doi.org/10.1016/0014-3057(89)90054-2).

- (28) Truong, N. P.; Jia, Z.; Burges, M.; McMillan, N. A. J.; Monteiro, M. J. Self-Catalyzed Degradation of Linear Cationic Poly(2-Dimethylaminoethyl Acrylate) in Water. *Biomacromolecules* **2011**, *12* (5), 1876–1882.

<https://doi.org/10.1021/bm200219e>.

### 3.5 Appendix



Appendix Figure 3.1: <sup>1</sup>H NMR of FFAm in CDCl<sub>3</sub> recorded at 600MHz